Final Technical Report: Impact of Wildfires on Solar Generation, Reserves, and Energy Prices

Mengmeng Cai,[1] Chin-An Lin,[1,2] Vikram Ravi,[1]
Yimin Zhang,[1] Cheng-Hsuan Lu,[2] and Manajit Sengupta[1]

1 National Renewable Energy Laboratory
2 University at Albany, State University of New York

NREL is a national laboratory of the U.S. Department of Energy
Office of Energy Efficiency & Renewable Energy
Operated by the Alliance for Sustainable Energy, LLC

This report is available at no cost from the National Renewable Energy Laboratory (NREL) at www.nrel.gov/publications.

Contract No. DE-AC36-08GO28308

Technical Report
NREL/TP-5D00-86640
June 2023

Final Technical Report: Impact of Wildfires on Solar Generation, Reserves, and Energy Prices

Mengmeng Cai,[1] Chin-An Lin,[1,2] Vikram Ravi,[1]
Yimin Zhang,[1] Cheng-Hsuan Lu,[2] and Manajit Sengupta[1]

1 National Renewable Energy Laboratory
2 University at Albany, State University of New York

Suggested Citation
Cai, Mengmeng, Chin-An Lin, Vikram Ravi, Yimin Zhang, Sarah Lu, and Manajit Sengupta. 2023. *Final Technical Report: Impact of Wildfires on Solar Generation, Reserves, and Energy Prices*. Golden, CO: National Renewable Energy Laboratory. NREL/TP-5D00-86640. https://www.nrel.gov/docs/fy23osti/86640.pdf.

NREL is a national laboratory of the U.S. Department of Energy
Office of Energy Efficiency & Renewable Energy
Operated by the Alliance for Sustainable Energy, LLC

This report is available at no cost from the National Renewable Energy Laboratory (NREL) at www.nrel.gov/publications.

Contract No. DE-AC36-08GO28308

Technical Report
NREL/TP-5D00-86640
June 2023

National Renewable Energy Laboratory
15013 Denver West Parkway
Golden, CO 80401
303-275-3000 • www.nrel.gov

NOTICE

This work was authored in part by the National Renewable Energy Laboratory, operated by Alliance for Sustainable Energy, LLC, for the U.S. Department of Energy (DOE) under Contract No. DE-AC36-08GO28308. Funding provided by U.S. Department of Energy Office of Energy Efficiency and Renewable Energy Solar Energy Technologies Office. The views expressed herein do not necessarily represent the views of the DOE or the U.S. Government.

Cover Photos by Dennis Schroeder: (clockwise, left to right) NREL 51934, NREL 45897, NREL 42160, NREL 45891, NREL 48097, NREL 46526.

Acknowledgments

We are grateful to the U.S. Department of Energy Office of Energy Efficiency and Renewable Energy Solar Energy Technologies Office. Specifically, we acknowledge Dr. Zachary Goff-Eldredge for his support and encouragement during this work.

We also thank several National Renewable Energy Laboratory researchers, including Dr. Aron Habte, Dr. Jaemo Yang, Mr. Marty Schwarz, Dr. Jiazi Zhang, and Dr. Garvin Heath.

List of Acronyms

ADS	Anchor Data Set
AERONET	Aerosol Robotic Network
AOD	aerosol optical depth
BA	Bay Area
BLM	U.S. Bureau of Land Management
CAISO	California Independent System Operator
CAL FIRE	California Department of Forestry and Fire Protection
CAS	California Shrub
CC	Central Coast
CESM	Community Earth System Model
CLM	Community Land Model
CMIP3	Coupled Model Intercomparison Project Phase 3
CONUS	contiguous United States
dGen	Distributed Generation Market Demand
DHI	diffuse horizontal irradiance
DNI	direct normal irradiance
DOD	U.S. Department of Defense
ECA	Eastern California
ESRL	Earth System Research Laboratory
FINN	Fire INventory from NCAR
FIRMS	Fire Information for Resource Management System
FTUV	Fast Tropospheric Ultraviolet-Visible
GeoMAC	Geospatial Multi-Agency Coordination
GHI	global horizontal irradiance
GOCART	Georgia Institute of Technology–Goddard Global Ozone Chemistry Aerosol Radiation and Transport
GOES	Geostationary Operational Environmental Satellite
IMS	Interactive Multisensor Snow and Ice Mapping System
LA	Los Angeles
LRA	Local responsibility areas
LSM	Land Surface Model
MBE	mean bias error
MEGAN	Model of Emissions of Gases and Aerosols from Nature
MERRA-2	Modern-Era Retrospective analysis for Research and Applications, Version 2
MODIS	Moderate Resolution Imaging Spectroradiometer
MOZART	Model for OZone and Related chemical Tracers
MOZCART	MOZART model coupled with GOCART model
NAM	North American Mesoscale
NASA	National Aeronautics and Space Administration
NCA	Northern California
NCAR	National Center for Atmospheric Research
NCV	Northern Central Valley
NEI	National Emissions Inventory
NIFC	National Interagency Fire Center

NOAA	National Oceanic and Atmospheric Administration
NPS	U.S. National Park Service
NSRDB	National Solar Radiation Database
OASIS	Open-Access Same-time Information System
PDT	Pacific Daily Time
PM	particulate matter
PNW	Pacific Northwest
PSM	Physical Solar Model
R	correlation coefficient
RCP	Representative Concentration Pathway
ReEDS	Regional Energy Deployment System
reV	Renewable Energy Potential
RMSE	root mean square error
RRTM	Rapid Radiative Transfer Model
SAM	System Advisor Model
SCA	Southern California
SCV	Southern Central Valley
SOLRAD	Solar Radiation
SPI	Standardized Precipitation Index
SRES	Special Report on Emission Scenarios
std	standard deviation
USF	U.S. Forest Service
USGS	U.S. Geological Survey
VLF	very large fire
WECC	Western Electricity Coordinating Council
WRAP	Western Regional Air Partnership
WRF	Weather Research and Forecasting
YSU	Yonsei University

Executive Summary

In the summer and early fall of 2020, large wildfires engulfed parts of Northern California, burned over 1 million acres and produced thick layers of smoke that blanketed large parts of the state. Although 2020 was a unique year in the last several decades, in terms of burn area, large wildfires and longer fire seasons are becoming more common with the changing climate. Thick smoke layers in the atmosphere can significantly attenuate solar radiation reaching solar arrays, and significantly reduce the electricity generated from those arrays.

In this study, we quantify the potential impacts of wildfires on the California grid. Specifically, we study the impacts under three different wildfire scenarios—a "no wildfire" scenario and two wildfire-specific scenarios, "2020 wildfire" and "enhanced wildfire" (with both scenarios assuming the same spatial distribution of the wildfire locations as the 2020 fires). We then combine each scenario with two solar energy infrastructure years, one corresponding to current solar deployment levels and one corresponding to the future (midcentury). This analysis is conducted using state-of-the-science modeling tools—primarily WRF-Chem for atmospheric modeling with chemistry to account for impacts of wildfires on solar radiation and PLEXOS for electricity market simulations.

Our analysis suggests that wildfires can significantly attenuate the solar radiation at both short downwind distances as well as far from emissions sources. WRF-Chem simulations indicate that monthly mean aerosol optical depth (AOD) increments averaged over the state can be as high as 0.14–0.46 (140%-460%), depending on the month of 2020, compared to a mean background AOD of ~0.10. Using PLEXOS simulations that account for impacts of change in AOD on photovoltaic (PV) generation, our analysis suggests that the 2020 wildfires resulted in a decrease of approximately 450 MW of generation on average in September 2020, the month with the most significant wildfire activity. Monthly PV generation decreased by 7.7% under current solar deployment levels, with additional possible reductions of 0.4% and 1.3% under the enhanced wildfire and increased PV deployment scenarios. Although the impacts of wildfires on PV generation are relatively small (~10% reduction, with PV representing 36% of the total installed capacity in 2036), they are not insignificant. Our analysis suggests that wildfire impacts on reserve requirements are much more pronounced. The 2020 wildfires scenario, and the enhanced wildfire scenario result in an increase in monthly reserve requirements of 53% and 64%, respectively. These levels of reduction in PV generation and enhancement in reserve requirements could likely increase the average price of electricity in the future if a wildfire situation similar to 2020 were to recur. It is also expected that there will be a much larger impact on price volatility.

Although our analysis is limited in scope, and the study considers only a few of the many factors that can affect PV generation and electricity markets, there is clear indication that wildfire smoke is an important factor that needs to be carefully considered and analyzed in planning the future grid.

Table of Contents

List of Figures

List of Tables

1 Introduction

1.1 Background

Wildfire activity has been increasing during the past few decades in the United States, and the importance of considering the impacts of wildfires on air quality and solar generation has also increased. Studying the various causes and effects of increasing wildfire activity has been the primary focus of several recent peer review studies (Abatzoglou and Williams 2016; Balch et al. 2017; Schoennagel et al. 2017; Seidl et al. 2017; Westerling 2016). For example, Abatzoglou and Williams (2016) used modeled climate projections to understand factors that affect the increase in wildfire activity and concluded that anthropogenic climate change accounted for approximately 55% of the observed increase in fuel aridity from 1979–2015 across the western United States. Similarly, Westerling (2016) analyzed the historic frequency of fire occurrences and showed that large wildfires (>400 hectare burn area) have been increasing since the 1970s, with approximately 20 additional large wildfires per decade in the western United States. This increased trend in fire severity and activity is predicted to continue in the next few decades. For example, Schoennagel et al. (2017) predicted that approximately 40% of the current wildland–urban interface is expected to experience a moderate to large increase in the probability of wildfires in the next 20 years, and the authors highlighted the risk to developed nonurban areas and infrastructure (e.g., solar power plants, power lines, pipelines).

Forest fires have a substantial influence on atmospheric aerosol loading and solar radiation because significant amounts of smoke aerosols emitted by wildfire activity can attenuate the solar radiation by absorption and scattering. This effect directly affects solar energy generation during fire episodes. Recent studies (Donaldson, Piper, and Jayaweera 2021; Gilletly, Jackson, and Staid 2021; Juliano et al. 2022) have investigated this phenomenon. Donaldson, Piper, and Jayaweera (2021) demonstrated that smoke aerosols emitted from wildfires can spread over vast areas, resulting in increased atmospheric aerosol loading and a significant decrease in solar radiation levels in California, United States, during the summer of 2020. Juliano et al. (2022) sought to quantify the impact of wildfires on solar energy by conducting numerical simulations using different aerosol optical depth (AOD) data sets (climatology and reanalysis with 3-hour variations) over the California Independent System Operator (CAISO) region in September 2020. Their findings indicated that smoke from wildfires led to a 10%–30% reduction of solar power production during peak hours (12−16 PDT in their study), and accounting for the changes in AOD caused by wildfires improved the solar energy forecast accuracy by nearly 50%. This substantial reduction of solar resource availability could introduce uncertainties and increase vulnerabilities in the solar energy market. As wildfire activity continues to increase, understanding the impact on solar energy availability and reserve requirements becomes increasingly crucial, particularly in high-solar energy penetration modeling scenarios. Hence, the accurate estimation of wildfire impacts is necessary for making informed decisions regarding reserve planning, generation scheduling, and reliability investments.

The objective of this project is to quantify the impact of wildfire-caused changes in atmospheric aerosol loading and thus on the availability of solar energy, ancillary services, and market prices for energy. An overview of various tasks in this project is shown in Figure 1. This assessment includes both a historical analysis and an estimation of future solar resource availability under different wildfire and solar penetration scenarios. It is expected that the study of wildfire impact on solar generation, reserve, and energy prices will provide useful information to system operators.

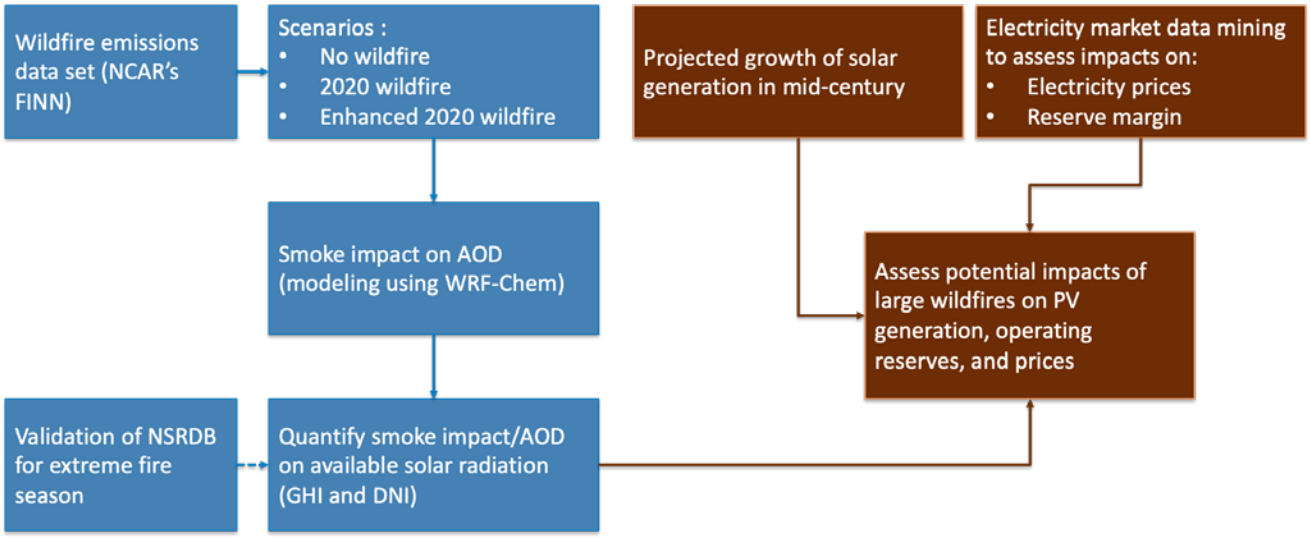

Figure 1. Overview of the project activities

1.2 Existing Work

Recent studies have explored the impacts of various meteorological extremes on electricity market operation. Jaglom et al. (2014) modeled the long-term energy, environmental, and economic impacts of rising temperatures caused by climate change on the U.S. power sector. A similar study was done by Hill et al. (2021), which focused on the West Coast region. Forrest et al. (2018) analyzed how droughts affect hydropower availability. The influence of extreme winter storms on wind power losses was explored in Akdemir, Kern, and Lamontagne (2022). Su et al. (2020) discussed how compound hydrometeorological extremes drive volatility in market prices and emissions. Zhao, Brooks, and Du (2021) provided an analysis summarizing the impact of hurricanes on a wholesale electricity market, using the Electric Reliability Council of Texas (ERCOT) as the example. Only a few studies, however (e.g., Gilletly, Jackson, and Staid [2021]), have focused on wildfires, and their analyses are limited to the impacts on solar generation. Moreover, most studies are conducted purely based on simulation data.

1.3 Limitations

Note that our emphasis is on the effects of wildfire-caused solar irradiance reduction. Other wildfire-caused damage—e.g., pertaining to transmission lines, substations, and power plants—are not within the scope of our study.

2 Evaluation of NSRDB Data and Development of Wildfire Scenarios

The following section provides a detailed description of various observational data sets and model products pertinent to wildfire attributes and solar radiation used in this study. Also included is a brief description of the methodology deployed to model changes in AOD under different scenarios. We use three different scenarios corresponding to three different levels of atmospheric aerosol loadings: one scenario corresponding to background aerosol levels and two wildfire-specific scenarios. These scenarios are described in detail in Section 2.2, Section 2.3, and Section 2.4.

2.1 Observational Data Sets and Model Products

2.1.1 Wildfire-Relevant Observational Data

To investigate the wildfire activity throughout the United States and its impact on the solar resource and solar markets, we collected wildfire-relevant data. We obtained wildfire data (acres of burned area, wildfire location, and period of wildfire) from geographic information system databases covering different periods of time: one from the U.S. Geological Survey (USGS)[1] (coverage years 2000–2019) and another from the National Interagency Fire Center (NIFC)[2] (coverage year 2020). The Geospatial Multi-Agency Coordination (GeoMAC)[3] web-based mapping application hosted by USGS was originally designed for fire managers to access information on current and historic fire locations, burn area, perimeter, ignition date, and control dates, harmonizing data from various sources, including Alaska Fire History Database, U.S. Department of Agriculture Forest Service regional fire history data, the U.S. Bureau of Land Management BLM fire planning and fuels management, the U.S. National Park Service (NPS), the U.S. Fish and Wildlife Service, the U.S. Bureau of Indian Affairs, and the California Department of Forestry and Fire Protection (CAL FIRE) Fire and Resource Assessment Program. It was made available to the public in 2000 and replaced by a newer application in 2020. The new application is hosted by the NIFC and is available at https://data-nifc.opendata.arcgis.com/. Because our analysis focused on the last 20 years (2000–2020), we combined data from both the NIFC repository and the 2020 parameters with the USGS data set to complete the data for the full 20-year period.

In addition, satellite-retrieved fire detection/hot spot data measured by Moderate Resolution Imaging Spectroradiometer (MODIS) were also used. MODIS are aboard National Aeronautics and Space Administration (NASA) Aqua and Terra polar-orbiting satellites measuring radiance near 11:30 and 13:30 local time. MODIS detects and identifies the pixel as occurrence of fire when the fire strength is sufficiently strong. Note that one wildfire event may include multiple fire detections/pixels depending on the size of wildfire. The fire

[1] See https://www.usgs.gov/.
[2] See https://data-nifc.opendata.arcgis.com/.
[3] See http://www.geomac.gov.

detection data are obtained from the NASA Fire Information for Resource Management System (FIRMS) website.[4]

2.1.2 Solar Radiation and Aerosol Optical Depth Observations

In this study, we used the ground-truth observation of Aerosol Robotic Network (AERONET) AOD and Solar Radiation (SOLRAD) to evaluate the National Solar Radiation Database (NSRDB) solar radiance and AOD data.

The AERONET project is a ground-based remote sensing network for the observation of aerosols (Holben et al. 1998). The temporal resolution of AERONET data is approximately 15 minutes, but it is irregular due to quality control (data during the maintenance of an instrument or with cloud contamination are removed). The Level 1.5 AOD data (cloud-screened and quality-controlled) collected from nine sites in California during 2018–2020 are used to evaluate the NSRDB. The AERONET AOD data were obtained from the NASA AERONET website.[5] The locations of the AERONET sites in California are shown in Figure 2.

The National Oceanic and Atmospheric Administration (NOAA) Earth System Research Laboratory (ESRL) SOLRAD Network monitors solar radiation over the United States and provides radiance data at a 1-minute frequency. We used solar radiation data measured at the Hanford site, including global horizontal irradiance (GHI), direct normal irradiance (DNI), and diffuse horizontal irradiance (DHI). The Hanford site, located in the central valley region of California in the city of Hanford, is the only SOLRAD site in the state of California (Figure 2). Detailed information on the NOAA SOLRAD Network can be found in Hicks, DeLuisi, and Matt (1996). SOLRAD radiation data were obtained from the NOAA ESRL SOLRAD website.[6]

[4] See https://firms.modaps.eosdis.nasa.gov/.
[5] See https://aeronet.gsfc.nasa.gov/.
[6] See https://www.esrl.noaa.gov/gmd/grad/solrad/.

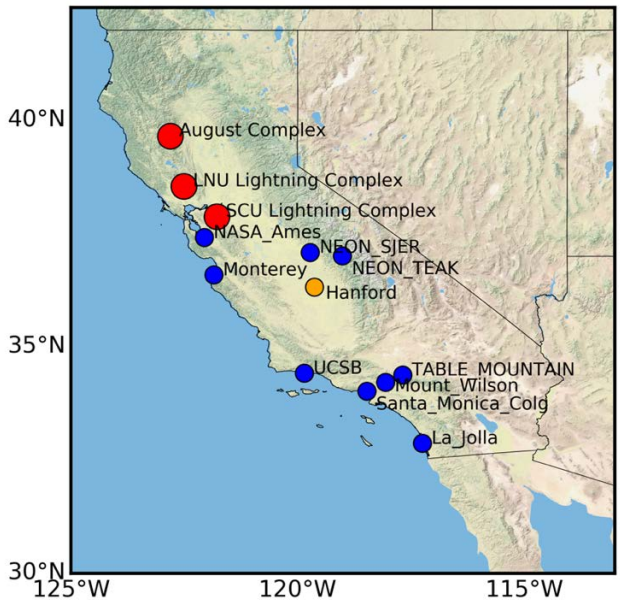

Figure 2. Locations of AERONET sites (blue circles), three of the largest fires in 2020 in California (red circles), and the solar radiation observation (yellow circles).

2.1.3 The National Solar Radiation Database (NSRDB)

The NSRDB data set was created by National Renewable Energy Laboratory (NREL) researchers and consists of solar radiation and meteorological conditions (Sengupta et al. 2018). For the coverage of North America, the NSRDB is simulated by NREL's Physical Solar Model (PSM) with the inputs of surface and atmospheric conditions from NOAA's Geostationary Operational Environmental Satellite (GOES), the National Ice Center's Interactive Multisensor Snow and Ice Mapping System (IMS), and NASA MODIS observations and Modern-Era Retrospective analysis for Research and Applications, Version 2 (MERRA-2) reanalysis (Sengupta et al. 2018). For the atmospheric aerosol information, the NSRDB AOD data were derived from MERRA-2 AOD and downscaled from the native resolution of the MERRA-2 (spatial resolution: 0.5° × 0.625° (50–67 km); temporal resolution: 1 hour) to the NSRDB resolution (spatial resolution: 2 km; temporal resolution: 5 minutes). The method of downscaling includes both spatial and temporal scaling algorithms. The solar radiation data from the NSRDB have been evaluated with surface measurements (Sengupta et al. 2018; Lin et al. 2023). Here, we used the solar irradiance (GHI and DNI), 2-m temperature, AOD, and cloud optical depth from the NSRDB[7] for the analysis.

Additionally, to investigate and quantify the wildfire impact for different scenarios, additional simulations for the no wildfire (background AOD) and enhanced wildfire scenarios were conducted using NREL's PSM. The model configuration is the same as that for simulating the NSRDB except for the AOD data. The methods to create the AOD data for the background AOD scenario and enhanced wildfire scenario are described in Section 2.3 and Section 2.4, respectively.

[7] The NSRDB data can be obtained from https://nsrdb.nrel.gov.

2.1.3.1 Evaluation of the NSRDB

NSRDB AOD and solar radiation data were evaluated with ground-based observations for both low and high fire activity periods. Because the temporal resolutions of the three data sets are different (NSRDB AOD and solar data: 5 minutes; AERONET AOD: approximately 15 minutes; SOLRAD solar data: 1 minute), we aligned the time stamp of the AOD and solar radiation data accordingly. For the AOD data, the 5-minute NSRDB AOD data with the nearest time stamp to the instantaneous AERONET AOD data were selected to match the time stamp of the AERONET data. For the solar radiation data, because the temporal resolution of the SOLRAD data (1 minute) is higher than that of the NSRDB data (5 minute), we selected the SOLRAD data at a 5-minute interval to match the temporal resolution of the NSRDB.

We focused on the period from 2018–2020 when the areas burned throughout California were reported as approximately 880,000, 140,000, and 1,440,000 acres in 2018, 2019, and 2020, respectively, according to CAL FIRE (CAL FIRE 2023). The years 2018 and 2020 had large wildfires in California, whereas the year 2019 had the lowest fire activity during the past decade; thus, we evaluated and compared the performance of the NSRDB AOD and solar radiation during the low fire activity period (July–November 2019) and the high fire activity period (July–November 2020). Statistical metrics, including root mean square error (RMSE), mean bias error (MBE), and correlation coefficient (R), were calculated to evaluate the accuracy of the NSRDB data.

Figure 3 shows scatterplots of the NSRDB AOD and AERONET AOD at the nine AERONET sites. The correlation coefficient of each site ranges from 0.57–0.81, and the RMSE ranges from 0.25–0.53. The MBE at all sites is small and ranges from -0.09–0.05. Table 1 shows the summary of the statistical metrics for the NSRDB AOD at the nine AERONET sites during the low fire activity period (July–November 2019) and the high fire activity period (July–November 2020). The mean AOD value across the AERONET sites is between 0.04–0.12 and 0.13–0.48 during the low fire activity period and the high fire activity period, respectively. The averaged MBE (0.01) and RMSE (0.04) during the low fire activity period is relatively small compared to that during the high fire activity period (MBE: –0.03; RMSE: 0.39). The negative MBE during the high fire activity period is probably due to the limitation of the downscaling algorithm coupled with the inadequacy of the aerosol transport model used by MERRA-2 to well capture the AOD value for extreme wildfire cases. The correlation coefficient during the high fire activity period (0.71) is higher than that during the low fire activity period (0.46). This is probably because the measurement of the low AOD has a higher uncertainty and the variation of the AOD is difficult to capture by a model under clean conditions (AOD <0.1). Randles et al. (2017) also reported that the MERRA-2 AOD exhibits a low correlation coefficient and a low bias against the observation over the remote Pacific, where the AOD is low (<0.3). Overall, MBE during the high fire activity period is comparable to that of the low fire activity period, and the full time series (2018–2020). The NSRDB also exhibits good performance in capturing the variation of AOD during the high fire activity period.

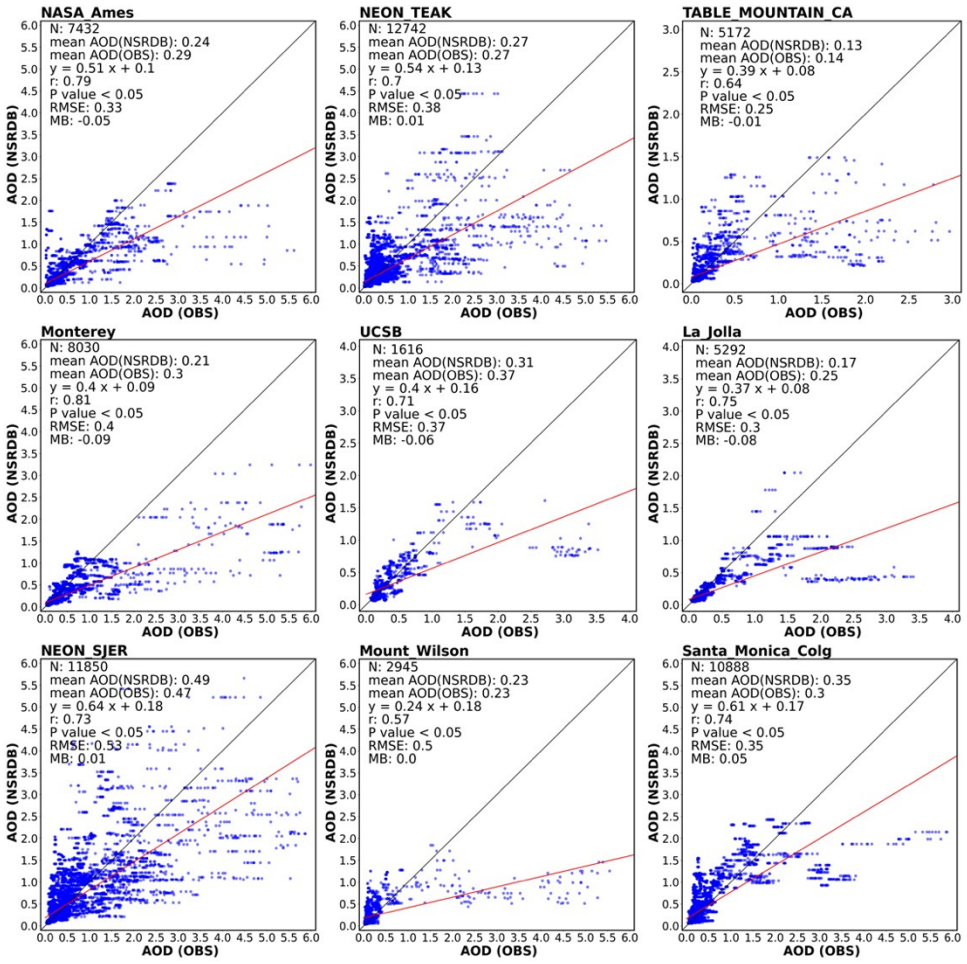

Figure 3. Scatterplots and metrics (RMSE, MBE, R) between the NSRDB AOD and AERONET AOD at nine sites from 2018–2020. The mean AOD of the NSRDB and AERONET and the number of samples (N) are also shown. The fitted linear model is shown in red, and the 1:1 slope line is shown in black.

Table 1. Summary of the Statistical Analysis (RMSE, MBE, R) of the NSRDB AOD at the AERONET Sites from July–November 2019 (Low Fire Activity Period) and July–November 2020 (High Fire Activity Period), Respectively

	July–November 2019 (Low Fire Activity Period)			July–November 2020 (High Fire Activity Period)		
Site	**MBE**	**RMSE**	**R**	**MBE**	**RMSE**	**R**
NASA Ames	-0.01	0.03	0.53	-0.05	0.34	0.78
Monterey	≈0	0.03	0.48	-0.09	0.42	0.78
NEON SJER	0.01	0.06	0.43	-0.06	0.54	0.72
NEON TEAK	0.01	0.03	0.5	-0.01	0.38	0.7
UCSB	0.03	0.04	0.68	-0.06	0.37	0.72
Mount Wilson	0.03	0.04	0.32	≈0	0.51	0.57
Table Mountain	≈0	0.02	0.49	-0.01	0.25	0.64
La Jolla	-0.01	0.04	0.25	-0.07	0.30	0.76
Santa Monica College	-0.01	0.05	0.44	0.04	0.37	0.72
Average	0.01	0.04	0.46	-0.03	0.39	0.71

NSRDB solar radiation data (GHI, DNI, and DHI) were evaluated with the SOLRAD observation at the Hanford site. Figure 4 shows the box plots of the GHI and DNI for the NSRDB and SOLRAD observation (OBS) at the Hanford site during 2018−2020. Results show that the median, 25th, and 75th percentiles of both NSRDB and the observations are comparable for GHI and DNI, indicating that the distribution of the two data sets is comparable. Statistical results show that the correlation coefficient of the GHI and DNI are high (≈ 0.9). RMSE of DNI (165.7 Wm^{-2}) is highest among all solar radiation variables, which is probably because DNI is more sensitive to the impact of aerosols than GHI (Sengupta and Wagner 2011). The GHI and DNI in NSRDB are overestimated, as shown by the MBE of 4.2 and 9.5 Wm^{-2}, respectively. Figure 5 shows the time series of the daily mean solar radiation during fire season (July–November) during 2018–2020 for SOLRAD and the NSRDB at the Hanford site. During the months with large fires in 2020 (August–October), both SOLRAD and the NSRDB show reductions in the daily GHI and DNI by up to approximately 200 Wm^{-2} and 400 Wm^{-2} in 2020 compared to the same period in 2019, indicating the attenuation effect of aerosols emitted from wildfires on solar radiation. The results also show that NSRDB can capture the impact of wildfire-driven aerosols on solar radiation.

Table 2 provides a summary of the statistical analysis (RMSE, MBE, R) of 5-minute solar radiation (GHI, DNI, DHI) from the NSRDB at the Hanford SOLRAD site during July–October 2019 (low fire activity period) and July–October 2020 (high fire activity period). Compared to the low fire activity period, the averaged GHI and DNI during high fire activity

period are reduced by approximately 30 Wm^{-2} and 90 Wm^{-2} (5.6 and 15.3%), respectively. The magnitude of the MBE of GHI and DNI in the high fire activity period is less than that in the low fire activity period (less than 10 Wm^{-2}); however, the RMSE of GHI, DNI, and DHI during the high fire activity period is much higher than that in low fire activity period, possibly due to the attenuation impact of wildfire activity on solar radiation. Further, the correlation coefficients of the GHI, DNI, and DHI are high (>0.85) during both fire activity periods, indicating that the NSRDB can well capture the variation of solar radiation. Overall, the MBE and the correlation coefficient of the NSRDB AOD and solar radiation during the high fire activity period are comparable to those during the low fire activity period. These evaluation results show that the NSRDB can well represent the impact of wildfires on the enhancement of AOD and the reduction of solar radiation; thus, the NSRDB and PSM are suitable approaches to be used for investigating and quantifying wildfire impact on solar radiation.

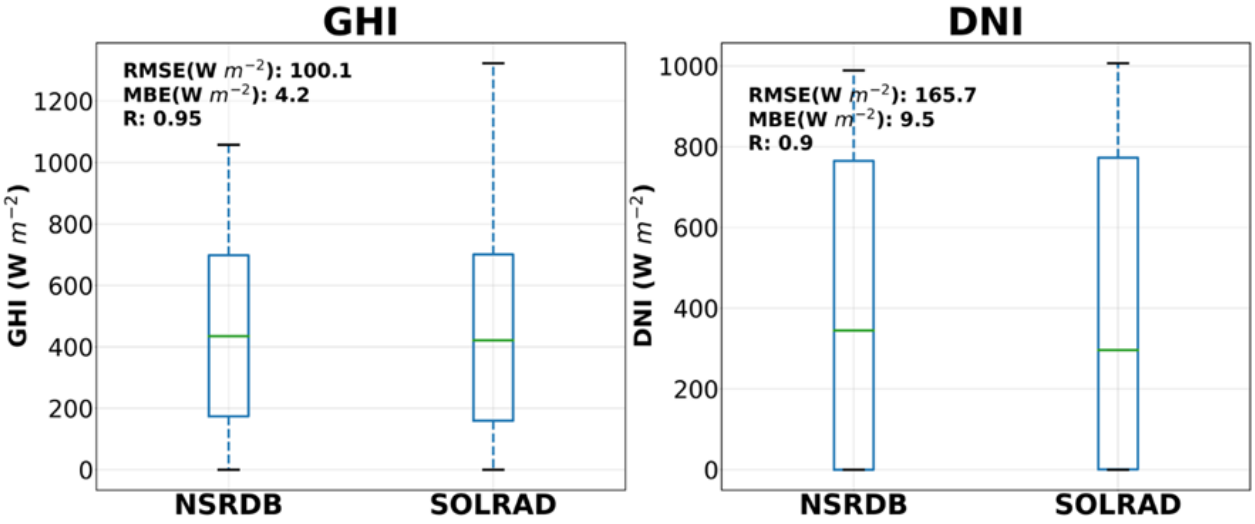

Figure 4. **Box plots of GHI and DNI for the NSRDB and SOLRAD observation (OBS) at the Hanford site during 2018–2020. For each box, the middle line and upper and lower hinges represent the median, the 25th (Q1), and the 75th (Q3) percentiles, respectively. The whiskers extend to 1.5 times the interquartile range (Q3–Q1), which is equal to 2.7 times the standard deviation. Metrics, including RMSE (unit: Wm^{-2}), MBE (unit: Wm^{-2}), and R of the NSRDB solar radiation, are calculated.**

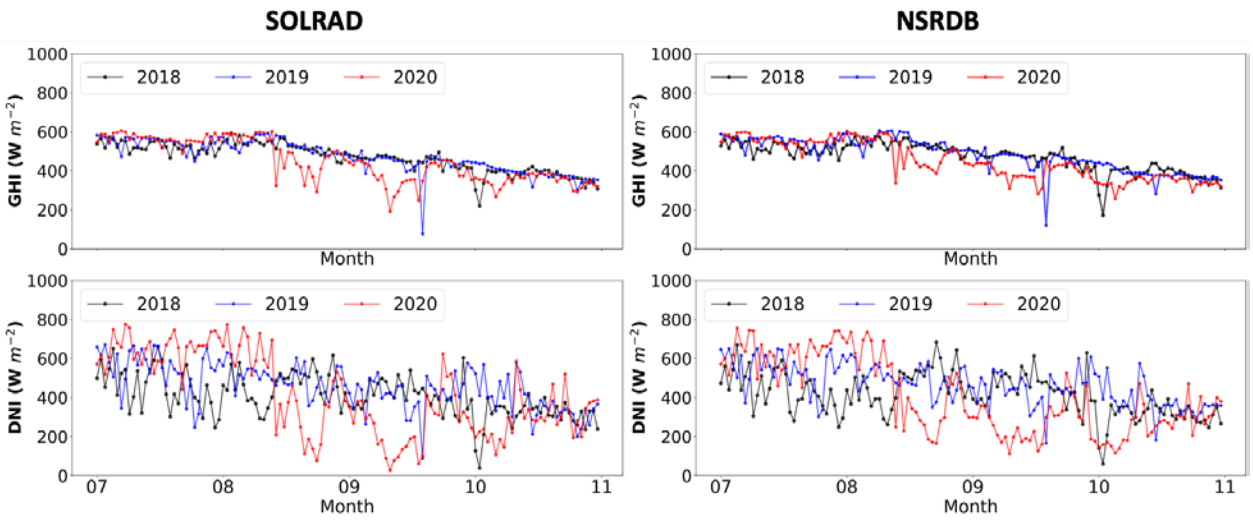

Figure 5. Time series of daily mean GHI and DNI during July–November 2018–2020 for the NSRDB and the SOLRAD (observation) Hanford site.

Table 2. Summary of Statistical Analysis (RMSE, MBE, R) of 5-Min Solar Radiation (GHI, DNI, DHI) From the NSRDB at the SOLRAD Hanford Site During July–October 2019 (Low Fire Activity Period) and July–October 2020 (High Fire Activity Period), Respectively

July–October 2019 (Low Fire Activity Period)					
Variable	MBE (Wm^{-2})	RMSE (Wm^{-2})	R	Average (SOLRAD)	Average (NSRDB)
GHI (Wm^{-2})	11.2	50.7	0.99	524	535
DNI (Wm^{-2})	14.0	107.4	0.95	558	572
DHI (Wm^{-2})	0.6	22.4	0.94	57	58
July–October 2020 (High Fire Activity Period)					
Variable	MBE (Wm^{-2})	RMSE (Wm^{-2})	R	Average (SOLRAD)	Average (NSRDB)
GHI (Wm^{-2})	3.1	91.9	0.95	494	497
DNI (Wm^{-2})	-6.5	172.2	0.86	481	475
DHI (Wm^{-2})	6.4	44.7	0.90	70	77

2.1.4 Atmospheric Modeling and Fire Emission Data

The WRF-Chem[8] model and the Fire Inventory from NCAR[9] (FINN) were used to create the AOD data set for the enhanced wildfire scenario. WRF-Chem Version 4.0 is a fully coupled meteorology-chemistry model. For this study, we selected the Model for OZone and Related chemical Tracers (MOZART) gas phase chemical scheme (Emmons et al.

[8] WRF-Chem: Weather Research and Forecasting Model with Chemistry
[9] NCAR: National Center for Atmospheric Research

2010) coupled with the Georgia Institute of Technology–Goddard Global Ozone Chemistry Aerosol Radiation and Transport (GOCART) aerosol scheme (Chin et al 2000), referred to as MOZCART (Pfister et al. 2011). Other parameterizations used include Thompson's microphysics scheme (Thompson, Rasmussen, and Manning 2004), the Rapid Radiative Transfer Model (RRTM) longwave (Mlawer et al. 1997) and Goddard shortwave radiation schemes (Chou and Suarez 1999), the revised Monin-Obukhov surface layer (Jiménez et al. 2012), the Noah-Land Surface Model (Noah-LSM), the Yonsei University (YSU) planetary boundary layer scheme (Hong, Noh, and Dudhia 2006), the Grell-Freitas cumulus scheme (Grell and Freitas 2014), and the fast Tropospheric Ultraviolet-Visible (FTUV) photolysis scheme. The National Centers for Environmental Prediction North American Mesoscale (NAM) 12-km analysis data[10] provided the initial and lateral boundary meteorological conditions. CAM-Chem model outputs provided the initial and lateral chemical conditions. Anthropogenic emissions for both area and point sources were obtained from the 12-km 2018 U.S. Environmental Protection Agency National Emissions Inventory (2018 NEI). Biogenic emissions were calculated online using the Model of Emissions of Gases and Aerosols from Nature (MEGAN) module (Guenther et al. 2006).

Biomass burning emissions were calculated using FINNv2.5 (Wiedinmyer et al. 2011). FINNv2.5 is based on fire counts derived from the MODIS. The hourly emissions are allocated using the standard Western Regional Air Partnership (WRAP) diurnal profile. For the enhanced wildfire scenario, FINN emissions were scaled and used to simulate AOD using WRF-Chem.

2.2 2020 Wildfire Scenario

First, we investigated the trend of wildfire activity over the United States from 2000–2020, as shown in Figure 6. There is significant interannual variability in the fire area burned; however, three of the largest fire years in the last 20 years occurred between 2015–2020, with the total burn area exceeding 10 million acres. It is also noteworthy that these same years are the largest fire years when considering fires larger than 10,000 acres, with approximately 200 fires occurring in 2015 and 2017 each but only 125 fires burning more than 10 million acres in 2020. This also highlights that 2020 was a somewhat unique year, considering that fewer fires contributed to a larger area burned. Given various studies that have indicated that future years are going to experience larger and more severe fires under climate change, considering 2020 as a base simulation year is likely to provide good insight into future wildfire impacts on atmospheric aerosol loading, which impacts solar resource availability. Further, a comparison among all states shows that California is the leading state where the burn area exceeded 1 million acres for 7 years from 2000–2020. Focusing on California, Figure 7 shows the yearly total fire detections for California during 2000–2020. The total fire detection for 2008, 2017, and 2018 show comparable values of approximately 20,000–25,000. The total fire detection in California in 2020 was much higher than that in 2017 and 2018 by a factor of 2–3, highlighting the potential of the impact of wildfire on solar radiation in California in 2020. Therefore, in this study, we

[10] See https://rda.ucar.edu/datasets/ds609.0/.

focused on the impact of wildfire activity on the solar resource and the solar market in California in 2020.

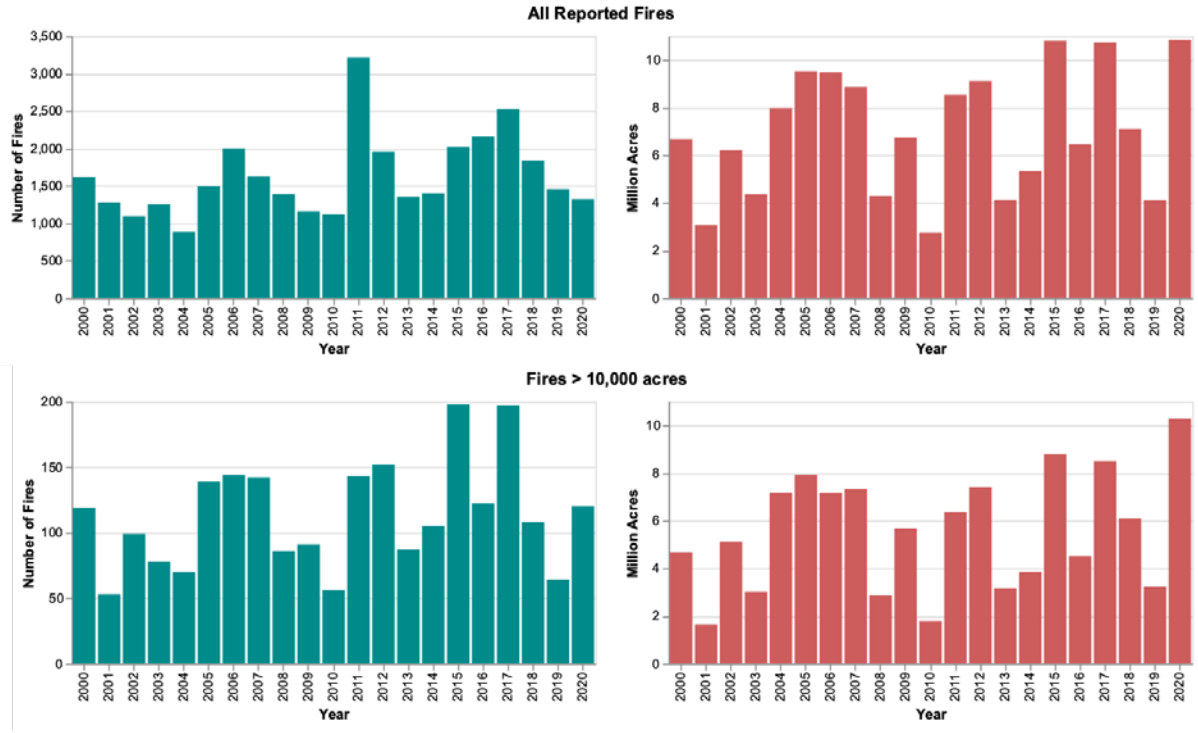

Figure 6. Yearly totals of wildfire events and acres burned between 2000–2020 as reported in the USGS and NIFC data sets. The top row shows the data for all reported fires, whereas the bottom row includes only fires that burned more than 10,000 acres.

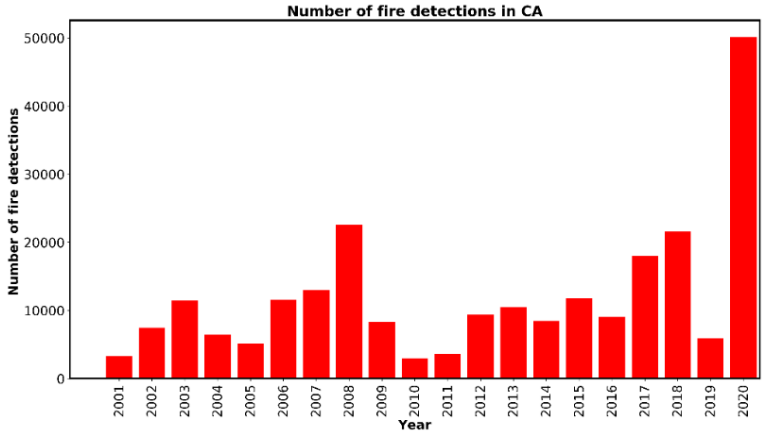

Figure 7. Total number of fire detections in California during 2000–2020.

2.3 Background AOD Scenario

To distinguish the background AOD and fire-affected AOD, MERRA-2 AOD data at a resolution of 0.5° × 0.625° during 2018 and 2020 were used to derive the map of the background AOD threshold. The threshold is determined as the median of the Gaussian mode $(m\mu) + 3 \times \text{standard deviation}\ (std)$ and is calculated for each grid. Figure 8a shows the probability density function of AOD at the NEON-SJER site during 2018–2020

as an example of determining the threshold. The AOD distribution (green shading) shows a right skewed distribution, where the high AOD is probably mainly attributed to wildfire smoke aerosols. First, we generated a smoothed nonparametric density distribution using Gaussian kernel (estimate mode; red solid line) and the AOD value of the peak of the estimate mode. With the assumption that the background AOD distribution is a normal distribution, a Gaussian mode of background AOD (cyan line) was empirically generated that best matched the original AOD data (green shading). Here, with the distance between zero and the AOD value at the peak of the estimate mode as 3 × std, the created Gaussian distribution covers the original AOD data most; thus, the threshold is determined as $m\mu + 3 \times std$ (blue line). Figure 8b shows the map of the background AOD threshold. The background AOD threshold is higher over the coastal area, Joaquin Valley, and Los Angeles, which might have more local pollutants than southeastern and northeastern California. Finally, to create the background AOD data set, the fire-affected AOD, identified as AOD values greater than the threshold, were replaced with $m\mu$. The background AOD data set at a resolution of 0.5° × 0.625° were then used for simulating the solar radiation for the no wildfire scenario using NREL's PSM.

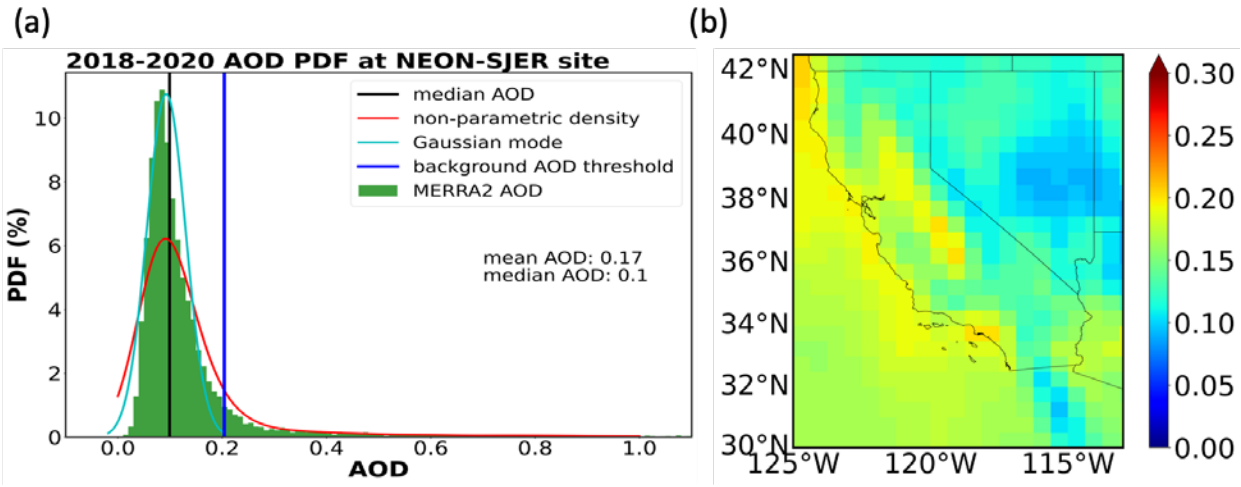

Figure 8. (a) Probability density function of AOD at the NEON-SJER site during 2018–2020. The median of all AOD data is indicated by the black solid line. (b) Map of background AOD threshold

2.4 Enhanced Wildfire Scenario

2.4.1 Projection of Wildfire Activity Based on Literature Review

Given drier and warmer weather conditions under an anthropogenic changing climate, wildfire activity is expected to increase in magnitude, length, and frequency (Westerling 2016; Abatzoglou and Williams 2016). With the input of simulated future meteorology from climate models, several studies have projected the fire activity over the western United States using statistical models (Spracklen et al. 2009; Yue et al. 2013; Yue, Mickley, and Logan 2014) or climate models coupled with land models (Ford et al. 2018; Li et al. 2020). Quantifying the increase of future fire severity and intensity, however, remains challenging due to complex and nonlinear interactions among weather, vegetation, and human activity (Brown, Hall, and Westerling 2004; Flannigan et al. 2009). There could be significant spatial variability with some areas of no change or even decreases in areas

burned and occurrences due to the differences in vegetation types. Additionally, the projected fire metrics are controlled by the selection of scenarios of future climate, including the Special Report on Emission Scenarios (SRES) and Representative Concentration Pathway (RCP) scenarios, and the predicted meteorology by climate models. Because modeling future climates and the impacts on fire-burned areas and consequent impacts on AOD is outside the scope of this study, here, we review previous studies and summarize the projected fire metrics, specifically around year 2050, and percentage increase relative to the present day. The consensus of the percentage increase of fire metrics, specifically the area burned and fire emissions, will be applied to the projected change in AOD and used to simulate their impact on the solar resource.

Most previous studies investigated wildfire projections for the future climate based on statistical models or physical land-based models. Statistical models regress the meteorological fields (e.g., temperature, wind speed, precipitation, relative humidity) to fire metrics (e.g., area burned, fire frequency, fire index) (Spracklen et al. 2009; Westerling et al. 2011; Yue et al. 2013; Yue, Mickley, and Logan 2014). Because wildfire events happen irregularly in space and time, statistical models for wildfire usually aggregate fire occurrences over space and/or time to provide some statistical smoothing of noisy data of the area burned. Further, because fire activity is closely related to the climate region and vegetation type, Spracklen et al. (2009) and Yue et al. (2013) divided the western United States into six ecoregions and built up the statistical model for each. California is covered by three main ecoregions, including the Pacific Northwest, California Coastal Shrub, and Desert Southwest. Spracklen et al. (2009) projected the area burned across the western United States to increase by 54% on average in the mid-21st century (Pacific Northwest: 78%; California Coastal Shrub: 38%). Yue et al. (2013) built their fire prediction model based on regression and parameterization. With an ensemble of 15 climate model runs from Coupled Model Intercomparison Project Phase 3 (CMIP3), Yue et al. (2013) showed that the area burned over the Pacific Northwest will increase by a factor of 42% (regression) or 156% (parameter). Over the California Coastal Shrub, the area burned will increase by a factor of 24% (regression). Considering the impact of elevation, population, fuel load, and the Santa Ana winds, Yue, Mickley, and Logan (2014) reported that the area burned will likely double in southwestern California and increase by 35% in the Sierra Nevada and 10% in central western California by the midcentury. Westerling et al. (2011) projected that the area burned over California under the SRES A2 and B1 scenarios will increase by ranges from 7%–41% in 2050. Instead of area burned, Barbero et al. (2015) projected an increase in the annual-mean number of very large fires (VLFs) by 62% over Mediterranean California and 300% over Western Cordillera during 2041–2070 under the RCP 8.5 scenario relative to present-day very large fires. Considering the anthropogenic influence (anthropogenic ignition and suppression), Mann et al. (2016) reported that the expected burned area will increase by 2%–5% over California by 2050. They also pointed out that previous findings of substantially increased numbers of fires and areas burned over California could be tied to omitted variable bias from the exclusion of human influences.

For studies based on land models, the Community Land Model (CLM) is widely used to simulate fire activity; it accounts for agricultural, deforestation, peat, and landscape fires, and it estimates the area burned and fire emissions using information about climate,

vegetation, land cover-land use changes, gross domestic product, and population density. By using climate models coupled with land models, area burned, or fire emissions can be derived at the climate model's grid cell resolution. Val Martin et al. (2015) used a global coupled chemistry–climate–land model called the Community Earth System Model (CESM) and CLM to project the future fire activity under RCP 4.5 and RCP 8.5 with climate, emissions, population, and land use changes. They reported increases in emissions in the western United States by approximately 100% in RCP 4.5 and 50% in RCP 8.5 by 2050. Pierce, Martin, and Heald (2017) used CESM-CLM with fire parametrization to project the area burned and showed that the area burned over the contiguous United States (CONUS) is expected to increase by 67% (RCP 4.5) and 50% (RCP 8.5). Following Pierce, Martin, and Heald (2017), Ford et al. (2018) investigated the change in the surface particulate matter ($PM_{2.5}$) for the early, mid, and late 21st century with both climate and population changes using CESM-CLM at a 0.9° × 1.25° horizontal resolution. They reported that smoke $PM_{2.5}$ emissions are expected to increase by 126% (RCP 4.5) and 54% (RCP 8.5) relative to present-day (2000–2010) smoke emissions over CONUS; however, the majority of the projected increase in smoke emissions is for the eastern United States (85% RCP 8.5, 220% RCP 4.5), not the western United States (40% RCP 8.5, 45% RCP 4.5). This is probably due to strong afforestation (more fuel) over the southeastern United States in the RCP 4.5 scenario and the increase in agricultural burning in the southeastern United States in the RCP 8.5 scenario. Because a reduction in the emissions of anthropogenic $PM_{2.5}$ is also considered, $PM_{2.5}$ concentrations are simulated to decrease in CONUS (total $PM_{2.5}$ decreases by 3% in RCP 8.5 and 34% in RCP 4.5 by 2100), but increasing fire-related $PM_{2.5}$ (fire-related $PM_{2.5}$ is projected to increase by 55% in RCP 4.5 and 190% in RCP 8.5 by 2100) are projected to offset these benefits and cause increases in total $PM_{2.5}$ in some regions. Li et al. (2020) used a dynamic vegetation model that includes a process-based representation of fire (LPJ-LMfire) with a global model (GEOS-Chem) to project fire emissions over the western United States under RCP 4.5 and RCP 8.5 and showed that emissions of smoke aerosols are expected to increase by 81% (RCP 4.5) and 86% (RCP 8.5) by 2050 relative to present-day emissions.

Overall, a literature review of previous studies on the projection of fire metrics under anthropogenic climate change is summarized in Table 3 and Figure 9. The projected relative increases of area burned and smoke emissions range from 2%–240% and 40%–100%, respectively, by 2050 among studies with different approaches and climate scenarios. Here, we chose the median (165%) among the reported increase ratios from the literature review as the increase ratio to scale the fire emission FINN data.

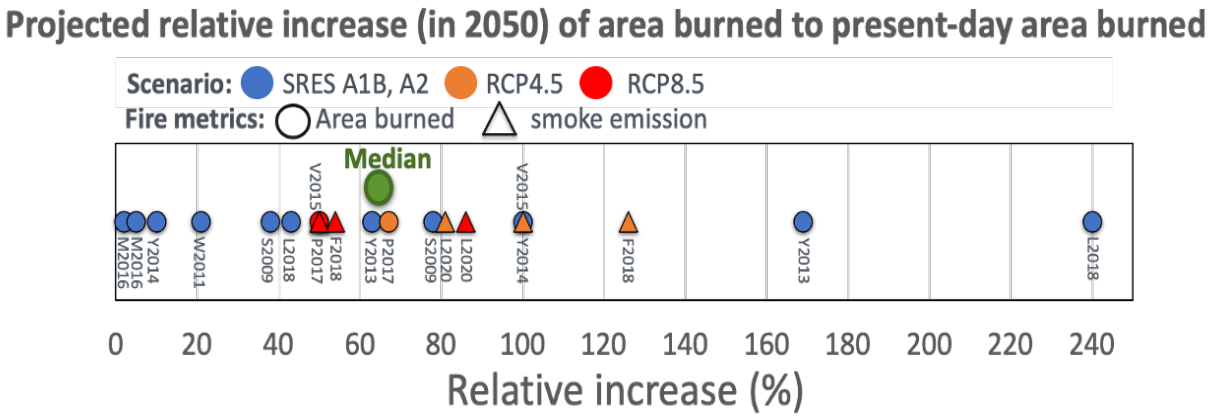

Figure 9. Summary of scatterplot of projected relative increase of area burned to present-day area burned from previous studies: Spracklen et al (2009): S2009; Westerling et al. (2011): W2011; Yue et al. (2013), Yue, Mickley, and Logan (2014): Y2013, Y2014; Val Martin et al. (2015): V2015; Mann et al. (2016): M2016; Pierce, Martin, Heald (2017): P2017; Ford et al. (2018): F2018; Littell et al. (2018): L2018; Li et al. (2020): L2020. Median increase (65%), which is the value used in this analysis, is also shown as a green circle.

Table 3. Review of Fire Predictions in the United States Under Future Climate Projections

VLF indicates very large fire; PNW: Pacific Northwest (ecoregion); CAS: California Shrub (ecoregion)

Reference	Method	Region, Scenarios, and Present/Future Time Slice	Fire Metric and Percentage Increase Relative to Present Day	Smoke PM and Percentage Increase Relative to Present Day
Spracklen et al. (2009)	Statistical model	Western United States, A1B, 1996–2005/2046–2055	Area burned: 38% (PNW[3]), 78% (CAS[4])	
Westerling et al. (2011)	Statistical model	California, A2 and B1, 1961–1990/2036-2065	Area burned: A1: 21%, B2: 23%	
Yue et al. (2013)	Statistical model + GEOS-Chem	Western United States, A1B, 1986–2000/ 2051– 2065	Area burned: 63%–169% Emissions of smoke aerosol: 150%–170%	Smoke PM concentration: 43%–55%
Yue, Mickley, and Logan (2014)	Statistical model	California, A1B, 1981–2000/2046–2065	Area burned: 10%–100%	
Barbero et al. (2015)	Statistical model	CONUS, RCP 8.5, 1971–2000/2041–2070	VLF[1]: 62% (Mediterranean California); 300% (Western Cordillera)	
Val Martin et al. (2015)	CLM-CESM	Western United States, RCP 4.5 and RCP 8.5, 2000/2050	Smoke PM emissions: RCP 4.5: 100%	Total PM2.5 concentrations: RCP 4.5: 22%

Reference	Method	Region, Scenarios, and Present/Future Time Slice	Fire Metric and Percentage Increase Relative to Present Day	Smoke PM and Percentage Increase Relative to Present Day
			RCP 8.5: 50%	RCP 8.5: 63%
Liu et al. (2016)	Statistical model + GEOS-Chem	Western United States, A1B, 2004–2009/2046–2051		Smoke PM concentration: 160%
Liu and Wimberly (2016)	Statistical model	Western United States, SRES A2, A1B, and B2, 1981–2010/ 2071–2100	Area burned: 28%–116%	
Mann et al. (2016)	Statistical model (+ human influence)	California, SRES A2, 1976–2000/2026–2050	Area burned: 2%–5%	
Pierce, Martin, and Heald (2017)	CLM + CESM	CONUS, RCP 4.5 and RCP 8.5, 1995–2005/2040–2050	Area burned: RCP 4.5: 67% RCP 8.5: 50%	Total PM2:5 concentrations: RCP 4.5: 146% RCP 8.5: 85%
Ford et al. (2018)	CLM + CESM	CONUS, RCP 4.5 and RCP 8.5, 2000–2010/2040–2050	Smoke PM emissions: RCP 4.5: 126% RCP 8.5: 54%	Total PM2:5 concentrations: RCP 4.5: 113% RCP 8.5: 27%
Littell et al. (2018)	Statistical model + climate model	Western United States, SRES A1B, 1980–2006/2030–2059	Area burned: 43%–240%	
Li et al. (2020)	LPJ-LMfire + GEOS-Chem	Western United States, RCP 4.5 and RCP 8.5, 2010/2050	Smoke PM emissions: RCP 4.5: 81% RCP 8.5: 86%	Smoke PM concentrations by 2100: RCP 4.5: 53% RCP 8.5: 109%
Liu et al. (2022)	Empirical fire model + climate model	Western United States, RCP 8.5, 2001–2010/2050–2059	Fire emissions: ~50%	
Dong et al. (2022)	Machine learning model (random forest)	Southern California, RCP 4.5 and RCP 8.5, 1970–1999/2070–2099	Large fire probability: RCP 4.5: 39% RCP 8.5: 62%	

2.4.2 AOD Data Set Creation Using WRF-Chem Modeling and MERRA-2 AOD

Because wildfire activity in 2020 is considered as the baseline year in this study, the enhanced fire emission FINN data was generated by applying the relative increase ratio to the original FINN in 2020. Therefore, we conducted two experiments at a resolution of 12 km using the original FINN (2020 wildfire) and enhanced FINN (enhanced wildfire) from June–November 2020. Note that we focused on wildfires in 2020, and only the area

burned was intensified. The locations and periods of wildfires remained the same as those in 2020.

The WRF-Chem simulated AOD for the 2020 wildfires were evaluated against the AERONET AOD observations and compared with the NSRDB AOD. For the WRF-Chem AOD, elevated AOD during August and September were captured, but the magnitude of the AOD was underestimated by approximately 1–2 when compared with the AERONET AOD. This could be a result of the coarse resolution of WRF-Chem in the spatial (12-km) and temporal (hourly) resolutions. Further, FINN, which is derived from satellite measurements of fire detections, could miss or underestimate wildfire emissions when there are clouds or thick smoke overlying the wildfires. In general, WRF-Chem can appropriately capture the major wildfire emission and represent the aerosol distribution.

Comparisons between the monthly spatial distributions of WRF-Chem AOD for the 2020 wildfire and enhanced wildfire scenarios are shown in Figure 10. During the low fire activity months (June and July), the spatial patterns of the AOD of the 2020 wildfire and enhanced wildfire conditions are similar, with AOD at most locations less than 0.5. For the high fire activity months (August–October), the enhanced AOD can be observed over Northern California and the San Joaquin Valley under the enhanced wildfire scenario. Especially during September, when an extreme wildfire event occurred, the AOD significantly increased, from approximately 0.5–1 to 1–2, over Northern California for the enhanced wildfire scenario. Because smoke aerosols emitted from wildfires can be transported by winds, intensified smoke aerosols lead to an increase in AOD over the San Joaquin Valley and most of the coastal area over Central California.

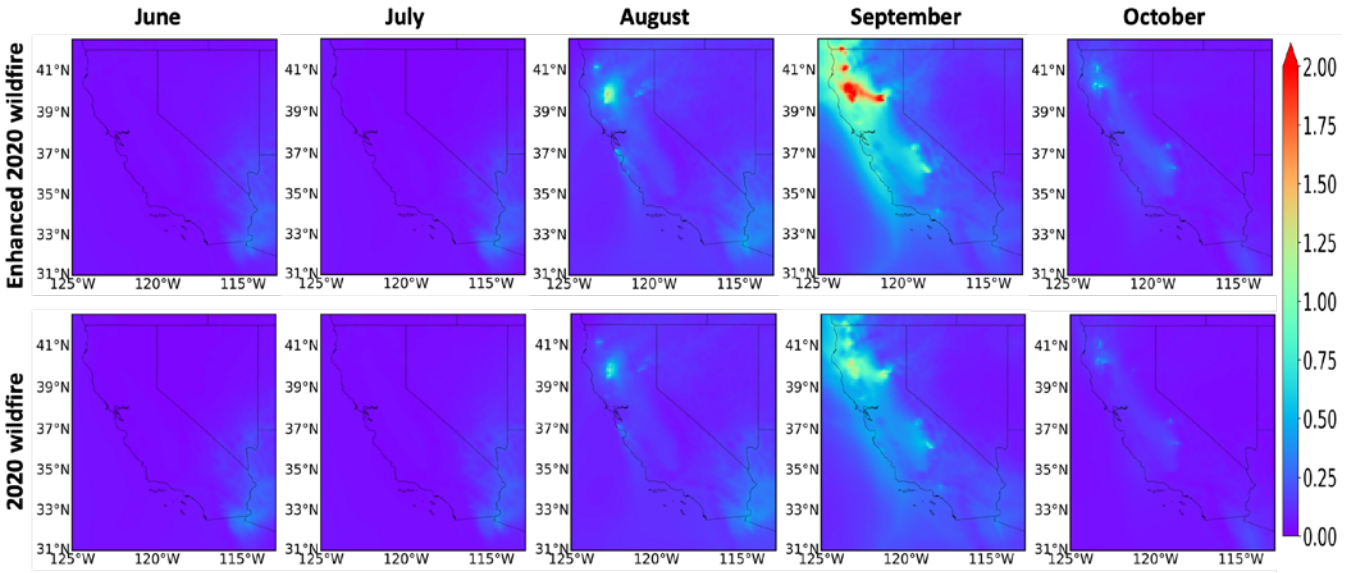

Figure 10. Monthly spatial distribution of AOD simulated by using WRF-Chem for the 2020 wildfire and enhanced wildfire scenarios.

Based on the two WRF-Chem simulations, we then derived the AOD increment map, defined as the difference between the enhanced wildfire AOD and the 2020 wildfire AOD. Because smoke aerosols emitted by wildfires can be transported by wind, the distribution

of the aerosols changes throughout the simulation period. To appropriately represent the impact of transported smoke aerosols on solar radiation, photovoltaic (PV) generation, and market prices, the AOD increment map was derived at a temporal resolution of 1 hour. However, due to the nonlinear effect of meteorology and chemical reactions, large differences of negative and positive AOD values between the 2020 wildfire and enhanced wildfire scenarios was found in the AOD map. This is probably because of the aerosol radiation effects on meteorology (especially for the boundary layer structure) and the distribution of aerosols, as well as the nonlinear impact of chemical reactions on the production of smoke aerosols. Therefore, we excluded the negative values of AOD increments to prevent generating negative value of AOD. Besides, we applied an upper limit of 10 to the AOD to prevent adding extreme large AOD increments to the NSRDB AOD. Finally, the AOD increments were applied to the 2020 NSRDB AOD to create the enhanced wildfire AOD data sets at the NSRDB resolution. Then, the enhanced wildfire AOD data set was used to simulated solar radiation using NREL's PSM.

3 Wildfire Impact on Aerosol Loading and Solar Radiation

3.1 Impacts During the 2020 Wildfire Scenario

To quantify the impact of wildfire activity on aerosol loading and solar radiation, we compared the differences of the simulated AOD and solar radiation between the no wildfire and 2020 wildfire scenarios while focusing on high fire activity months (August, September, and October). Figure 11 shows the box/whisker plots of the monthly AOD over California for the no wildfire and 2020 wildfire scenarios. The monthly mean AOD is approximately 0.06 during August and October for the no wildfire scenario. With the smoke aerosols emitted from wildfires, the AOD increases by 0.14–0.46 in the 2020 wildfire scenario. The AOD increases the most in September, with a monthly mean AOD of 0.53. Further, the distribution of the AOD is wider under the 2020 wildfire scenario than under the no wildfire scenario, indicating a larger variation of the spatial distribution of AOD over California.

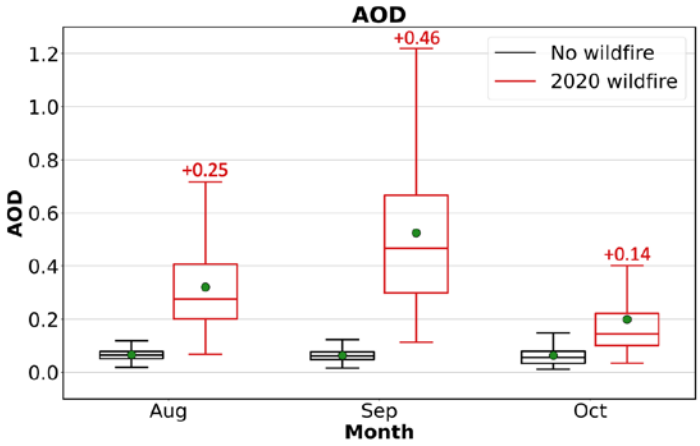

Figure 11. Box/whisker plot of monthly AOD over all grid cells in California for the no wildfire and 2020 wildfire scenarios. For each box, the middle line, green dot, and upper and lower hinges represent the median, mean, and 25th (Q1) and 75th (Q3) percentiles, respectively. The whiskers extend to 1.5 times the interquartile range (Q3–Q1), which is equal to 2.7 times the standard deviation. The difference in the monthly mean AOD between the two scenarios is also shown (red font).

Regarding the wildfire impact on solar radiation, comparisons of GHI, clear-sky GHI, DNI, and clear-sky DNI between the no wildfire and 2020 wildfire scenarios are shown in Figure 12. Note that the solar radiation data selected for analysis included only the period from 10 a.m.–6 p.m. local time (Pacific Daylight Time [PDT]). Clear-sky GHI and clear-sky DNI are also shown to exclude the impact of clouds and to highlight the aerosol impact on solar radiation. Because GHI consists of DNI and DHI, solar radiation scattered by atmospheric aerosols can increase DHI and then contribute to GHI. Therefore, wildfire-caused changes in AOD showed a moderate impact on monthly GHI and lead to a reduction in monthly GHI by 2.9%–6.9%. The aerosol impact on clear-sky GHI was slightly stronger than that on GHI and caused a reduction in clear-sky GHI by 3.3%–7.9%. The largest reduction in GHI and clear-sky GHI occurred in September, when the AOD

increased the most. Because DNI is more sensitive to the attenuation effect of atmospheric aerosols, the aerosol impact on DNI was more significant than that on GHI. The enhanced aerosol loading led to a reduction in the monthly mean DNI and clear-sky DNI by 73–188 Wm^{-2} (9.3%–22.7%) and by 85–221 Wm^{-2} (10.1%–24.9%) over California, respectively. Overall, with the intense aerosol loading under the 2020 wildfire scenario, GHI and DNI can be reduced by up to approximately 7% and 23%, respectively. This profound reduction of the available solar radiation can potentially influence solar PV generation, grid stability, and market price.

Multiple factors, including locations of wildfires, injection height, and synoptic wind fields, can affect the distribution of smoke aerosols emitted from wildfires and thus its impact on solar radiation. Figure 13 shows the spatial pattern of the differences in the monthly AOD and DNI between the 2020 wildfire and no wildfire scenarios from August to October. Because most of the large wildfires occurred over Northern California, a profound monthly AOD difference can be found over Northern California, with increases of AOD greater than one during August and September. A considerable AOD increase can be also observed over the Central Valley in September and October, possibly due to nearby wildfires and the transport of smoke aerosols to areas downwind from Northern California. Further, the geographic impact of the valley can restrict the dispersion of atmospheric aerosols and lead to an accumulation of aerosols and high AOD. The wildfire activities show a moderate impact on the increase of AOD over Southern California and southeastern California, which are relatively far from the location of large wildfires. Regarding the wildfire impact on DNI, a significant decrease in DNI can be found over the areas with large increases in AOD; this corresponds to a monthly reduction in DNI by up to 200 Wm^{-2}. Note that the exponential attenuation effect of AOD on DNI could lead to a pronounced impact on the reduction in DNI, which occurred in areas with moderate AOD changes. For instance, with an increase in the monthly AOD of 0.4–0.5 over the Los Angeles metropolitan area, the magnitude of the DNI reduction is comparable (150–200 Wm^{-2}) to that over the source region, where AOD increased by more than one due to wildfire impacts.

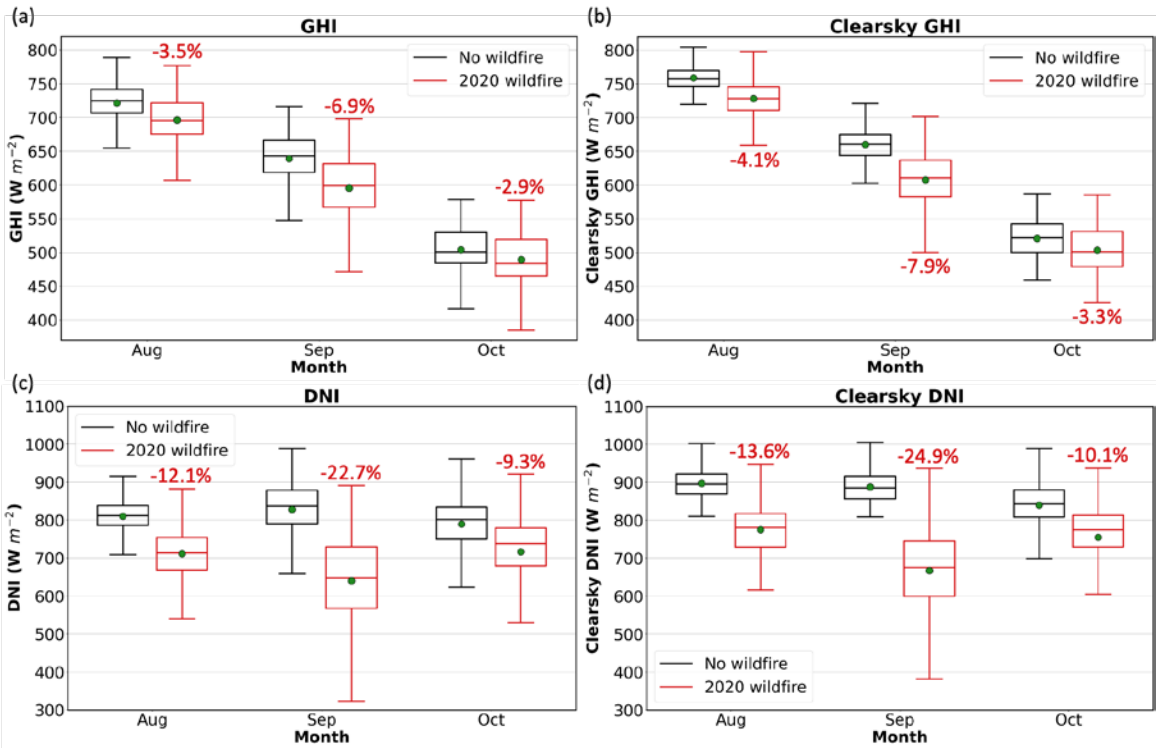

Figure 12. Box/whisker plots of monthly solar radiation, including (a) GHI and (b) clear-sky GHI, (c) DNI, and (d) clear-sky DNI, over all grid cells in California for the no wildfire and 2020 wildfire scenarios. The relative difference in the monthly mean solar radiation between the two scenarios is also shown. The green dot indicates the monthly mean value of the solar radiation.

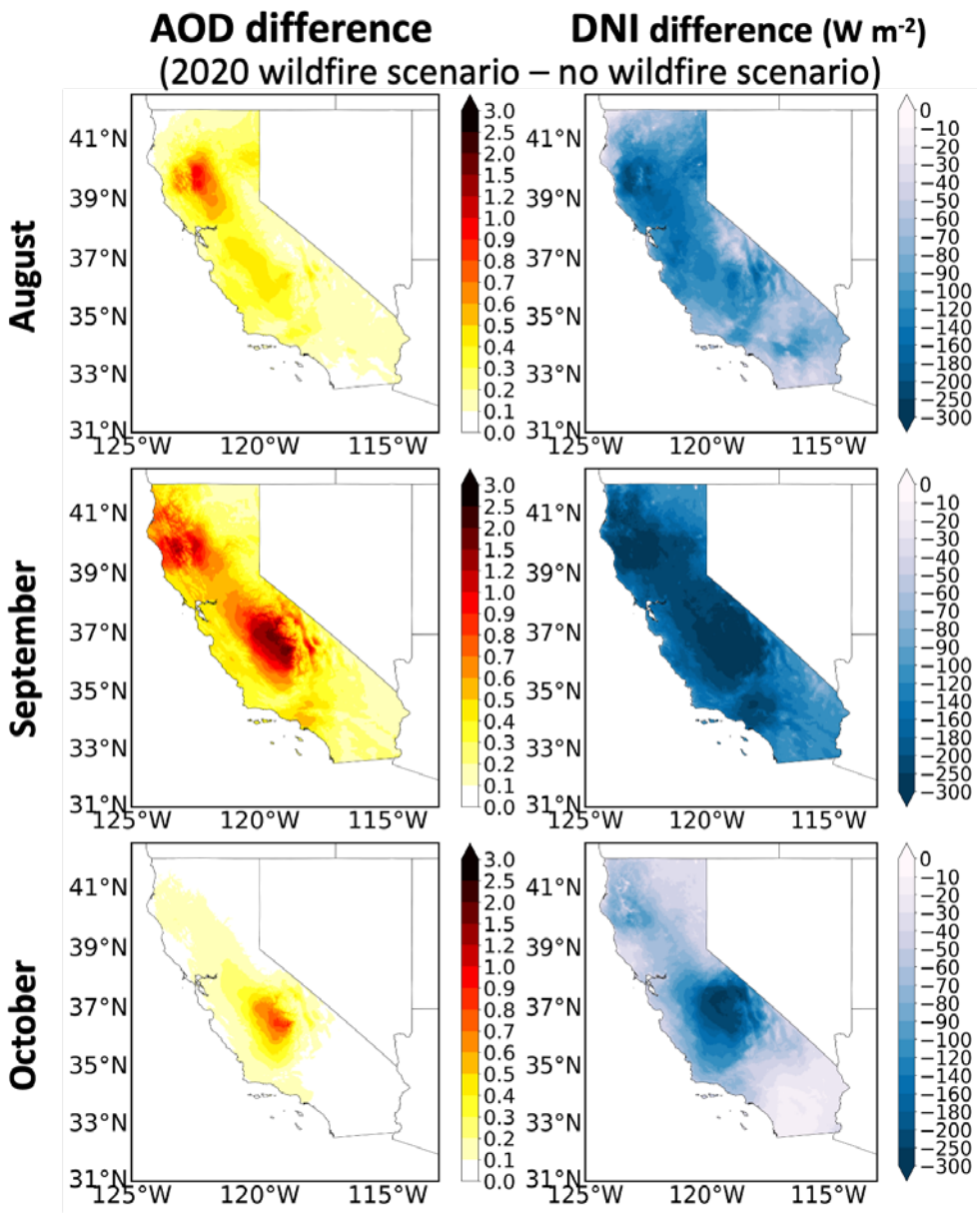

Figure 13. Spatial pattern of the difference in the monthly AOD and monthly DNI between the 2020 wildfire and the no wildfire scenarios from August–October. DNI was selected only for the period from 10 a.m.–6 p.m. local time (PDT).

To study the profound spatial variation of wildfire impact, we further focused on eight selected subregions, as shown in Figure 14, to better quantify the wildfire impact on aerosol loading and solar radiation availability. In addition, we analyzed the wildfire impact at a shorter time interval (daily) because atmospheric aerosols could be transported by wind and exhibit large variations in daily aerosol loading. Figure 15 shows the box/whisker plot of the difference in the domain-averaged daily AOD and DNI between the 2020 wildfire and no wildfire scenarios for the eight subregions from August–October. As shown in Figure 15, the extensive range between the upper and lower whiskers of the differences between the AOD and DNI indicate distinct daily variations in aerosol loading and its impact on DNI. During August and September, the upper whiskers show daily AOD

increases of approximately 1.0–1.8 for subregions near the source and coastal areas (Northern California, Bay Area, Northern/Southern Central Valley, and Central Coast) during the days with severe wildfire impacts. This enhanced AOD can lead to significant reductions in the daily DNI by up to 300–500 Wm^{-2} (approximately 30–50%). This large sudden decrease in the available solar radiation can affect solar PV production and introduce uncertainties and vulnerabilities to electric grid stability. In the southern part of California, Los Angeles is also under the considerable influence of AOD and DNI impacts in September due to the transport of smoke aerosols. Overall, the impact of enhanced fire activity on DNI could be stronger on shorter (daily) timescales and in smaller domains, and the impacts can significantly vary by subregion.

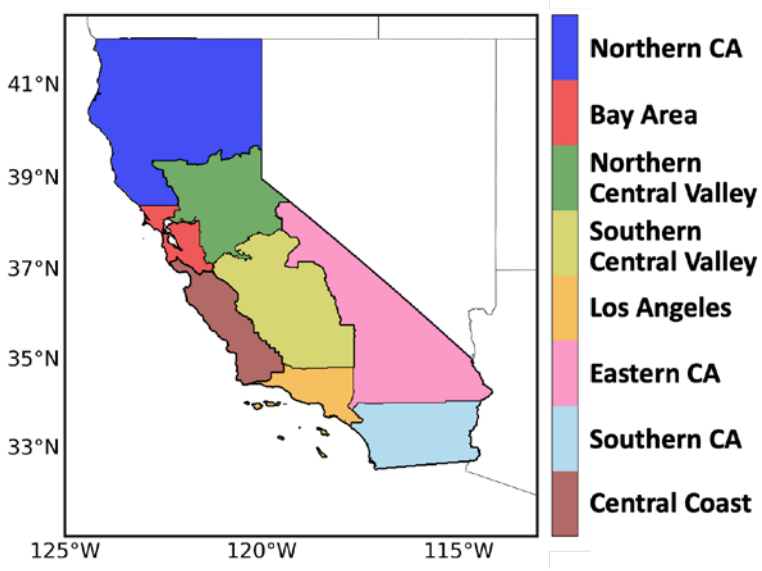

Figure 14. Map of eight focused subregions in California.

The map is adapted from the California electricity demand forecast zone map (total of 25 zones). Accessed June 29, 2023. https://cecgis-caenergy.opendata.arcgis.com/datasets/86fef50f6f344fabbe545e58aec83edd/explore.

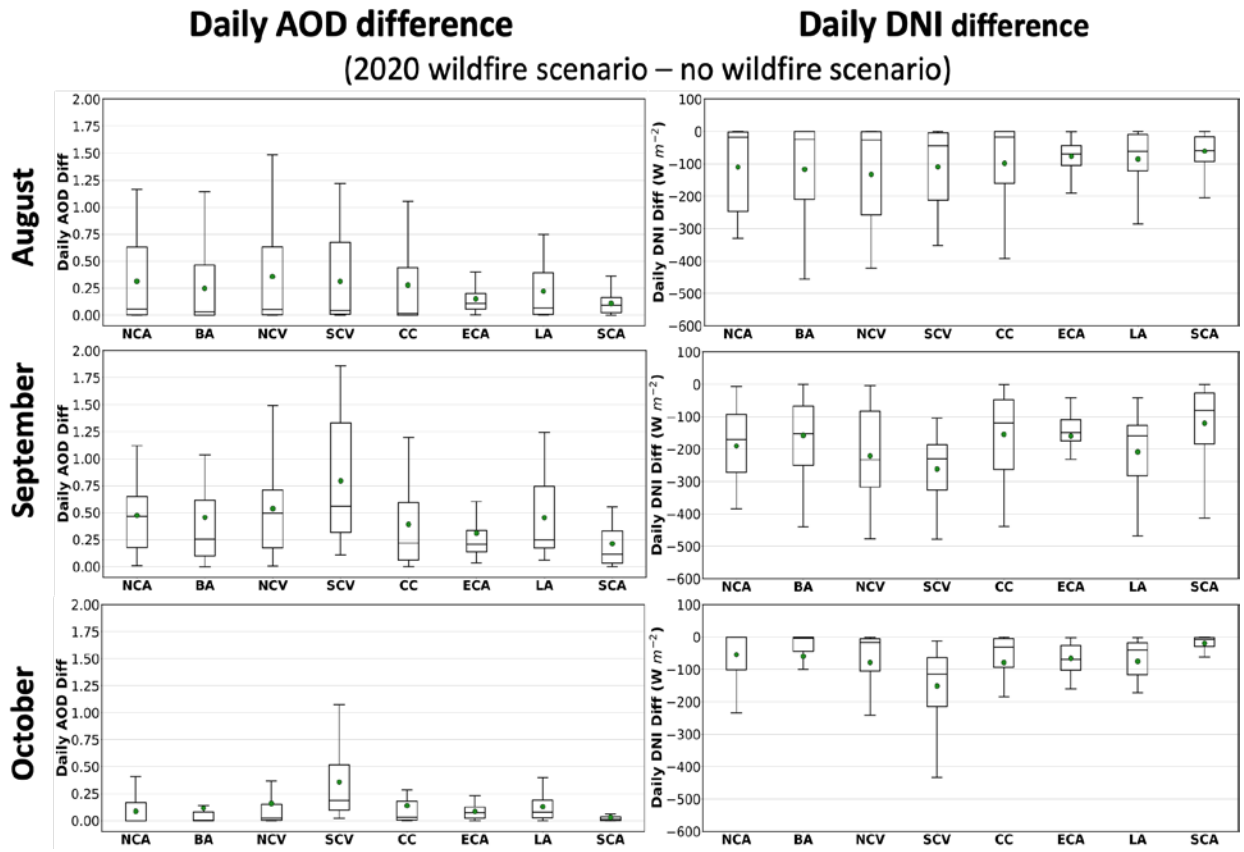

Figure 15. Box/whisker plots of domain-averaged differences in daily AOD and DNI between the 2020 wildfire and no wildfire scenarios for eight subregions from August–October. The green dot indicates the average of the daily AOD difference and DNI difference. DNI was selected only for the period from 10 a.m.–6 p.m. local time (PDT) to calculate the daily DNI.

NCA: Northern California; BA: Bay Area; NCV: Northern Central Valley; SCV: Southern Central Valley; CC: Central Coast; ECA: Eastern California; LA: Los Angeles; SCA: Southern California

3.2 Impacts During the Enhanced Wildfire Scenario

The spatial pattern of the monthly difference in the AOD and DNI between the enhanced wildfire scenario and the 2020 wildfire scenario is shown in Figure 16. Because most large wildfires in 2020 occurred over Northern California, enhanced AOD can be found over Northern California in the enhanced wildfire scenario, especially in September. The result shows that AOD increases by approximately 1–1.5 over the source region (Northern California). Further, these smoke aerosols can be transported by synoptic winds and lead to an increase in AOD of approximately 0.2–0.5 over downwind areas, such as San Joaquin Valley, Bay Area, and even the coastal areas near Los Angeles. This enhanced AOD can lead to reductions in DNI across the state; the reduction in the monthly DNI is up to 100 Wm^{-2} over the source region and approximately 30–70 Wm^{-2} over downwind areas. A pronounced enhanced wildfire impact on the reduction in DNI was observed not only over Northern California but also southwestern California, where the AOD difference is relatively low. This is because of the exponential attenuation effect of AOD on DNI that smoke impact on the reduction of solar irradiance could be even comparable over source and downwind area.

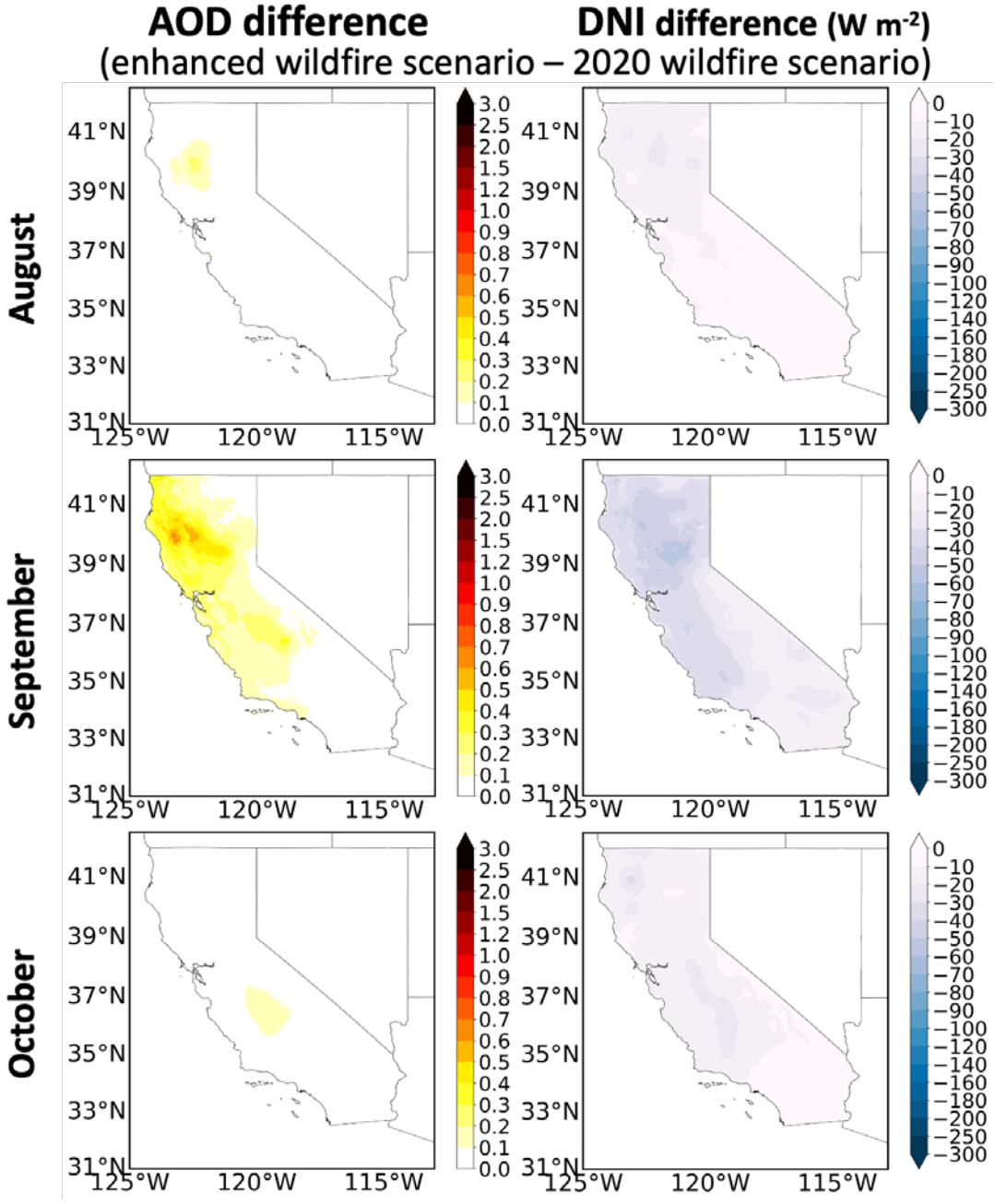

Figure 16. Spatial pattern showing the difference in monthly AOD and monthly DNI between the 2020 wildfire and no wildfire scenarios from August–October. DNI was selected only for the period from 10 a.m.–6 p.m. local time (PDT).

To quantify the impact of enhanced wildfire activity on AOD and solar radiation, Figure 17 shows the box and whisker plots of monthly AOD and clear-sky GHI over all grid cells in California for the no wildfire, 2020 wildfire, and enhanced wildfire scenarios. Because PV panels can generate solar energy using not only DNI but also GHI, here, we focused on clear-sky GHI. (The wildfire intensity index based on clear-sky GHI is defined and used in the next section for market analysis.) Compared to the background AOD, wildfires lead to an increase in the monthly mean AOD by approximately 0.2–0.7 for the enhanced

wildfire scenarios. Compared to the 2020 wildfire AOD, AOD for the enhanced wildfire case increases by approximately 11%–28% and shows a larger spread of AOD values. The enhanced AOD is expected to cause a reduction in solar radiation. For the clear-sky GHI, the reductions in clear-sky GHI under the 2020 wildfire and enhanced wildfire conditions are comparable. Compared to no wildfire condition, wildfire impact leads to reduction in clear-sky GHI by 3.4–7.9% in the 2020 scenario and 3.9–9.3% in the enhanced wildfire scenario over California. The enhanced wildfire scenario impact on GHI is less significant than that on AOD, which is probably due to the exponential attenuation effect of AOD on solar radiation ($GHI = GHI_{initial}\ e^{-AOD}$). Because the AOD in 2020 is already high over California, the statewide impact of the enhanced wildfire activity is only moderate.

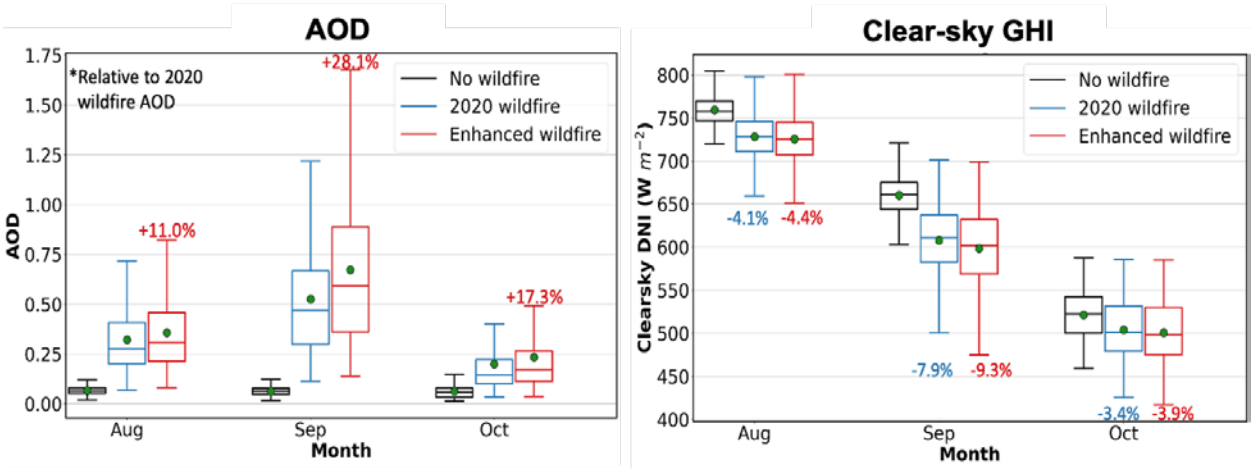

Figure 17. Box/whisker plots of monthly AOD and clear-sky GHI over all grid cells in California for the no wildfire, 2020 wildfire, and enhanced wildfire scenarios. The relative differences in the monthly mean AOD and clear-sky GHI are also shown. The green dot indicates the monthly mean values. Note that clear-sky GHI were selected only for the period from 10 a.m.–6 p.m. local time (PDT).

Because the wildfire impact on AOD and solar radiation exhibits large spatial and temporal variability, we further analyzed its impact by focusing on a smaller domain and a shorted period. Two regions were selected as examples: one near the source area (Greater Bay area) and a downwind area (Los Angeles metropolitan area) (Figure 14). Figure 18 shows the box and whisker plots of the daily clear-sky GHI over all grid cells for the Greater Bay and Los Angeles metropolitan areas in California for the no wildfire, 2020 wildfire, and enhanced wildfire scenarios during the wildfire episode (September 10–September 14). First, for the 2020 wildfire scenario, compared to the no wildfire condition, the impact of the 2020 wildfire leads to a decrease in clear-sky GHI by up to 23% (near the source) and 19% (downwind). The impact of the enhanced wildfire activity further intensifies the reduction in clear-sky GHI; it has a stronger impact near the source area, which leads to a reduction by up to 30% (near the source), and it has a moderate impact on the downwind area. Compared to the monthly statewide wildfire impact, the daily zone-level wildfire impact on solar radiation is much more significant. This impact could be even stronger for shorter periods (e.g., hourly), and this sudden reduction of solar radiation could introduce uncertainties and vulnerabilities to grid stability.

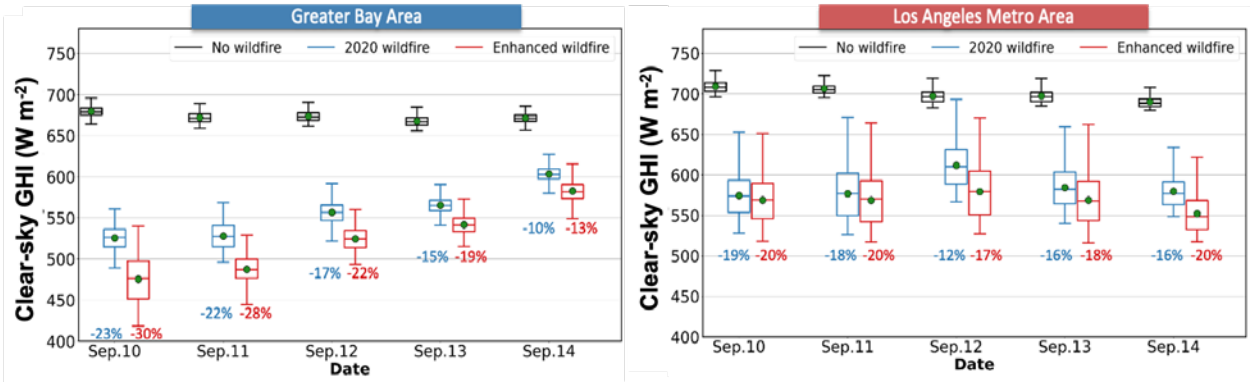

Figure 18. Box/whisker plots of daily clear-sky GHI over all grid cells for the Greater Bay and Los Angeles metropolitan areas in California for the no wildfire, 2020 wildfire, and enhanced wildfire scenarios. The relative differences in the monthly mean AOD and clear-sky GHI are also shown. The green dot indicates the monthly mean values. Note that clear-sky GHI were selected only for the period from 10 a.m.–6 p.m. local time (PDT).

4 Market Impact Analysis: Real-World Data Mining

With the bulk grid increasingly relying on solar generation, wildfires could introduce significant variability and uncertainty of energy availability and make the power system more vulnerable to reliability issues and market price volatility. To make informed decisions on reserve planning, generation scheduling, and reliability investments to mitigate the influences of wildfires, the first step is to understand how wildfires have historically impacted the electricity market. Therefore, as the first part of our wildfire market impact study, we present a historical wildfire market impact analysis leveraging real-world historical data.

4.1 Data Preparation

The process of conducting the historical wildfire-market impact analysis heavily relies on the availability of relevant data. As such, we dedicate a subsection to discuss the data preparation and properties. We collected three types of real-world data sets to support the analysis: meteorological, wildfire, and market data sets, as described in sections 4.1.1, 4.1.2 and 4.1.3, respectively.

4.1.1 Solar Irradiance and AOD Data

The solar irradiance data are provided by the NSRDB,[11] which was developed at NREL. The database offers a variety of solar radiation data—including GHI, DNI, and DHI—at high resolutions in both time (15-minute intervals) and space (2 km × 2 km), incorporating satellite measurements, ground-based measurements, and model-based data. Details can be found in Section 2.1.3.

4.1.2 Wildfire-Relevant Data

Table 4 summarizes the wildfire-relevant data sets used in the analysis according to data type, data source, spatial precision, temporal precision, and magnitude measure/unit. Two types of wildfire-relevant data—wildfire records and clear-sky GHI—were applied to serve as direct and indirect measures of the wildfire, respectively.

Table 4. Wildfire-Relevant Data Sets

Data Type	Data Source	Spatial Precision	Temporal Precision	Magnitude Measure/unit
Wildfire records	Fire agencies: NIFC, DOD, LRA, USF, NPS, BLM[a]	Latitude and longitude of the fire perimeter centroid	Start date and end date	Burn area (acres)
Clear-sky GHI	NSRDB	2-km x 2-km grid	15 min	(Wm^{-2})

NIFC: National Interagency Fire Center, DOD: U.S. Department of Defense, LRA: Local responsibility areas, USF: U.S. Forest Service, NPS: U.S. National Park Service, BLM: U.S. Bureau of Land Management

[11] See https://nsrdb.nrel.gov.

As described in Section 2.1.1, wildfire records were obtained from NIFC and USGS. For the analysis on the impact of wildfire activity on market price, we focused on the period from 2017–2020.

Figure 19 shows the monthly burn areas across 4 years (2017–2020), calculated based on the historical wildfire records. Then we filtered out months with burn areas that exceeded 0.2 million acres, as listed in Table 5. According to Figure 19 and Table 5, most wildfires in California occurred during the second half of the year, and the months with greater wildfire impact slightly vary across years.

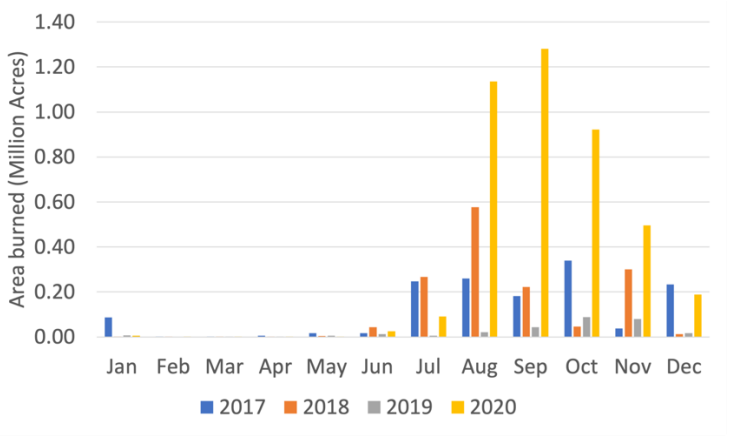

Figure 19. Monthly burn areas

Table 5. Months With Burn Areas Greater Than 0.2 Million Acres

Year	Months with Burn Areas Greater Than 0.2 Million Acres
2017	July, August, October, December
2018	July, August, September, November
2019	*No month exceeded the threshold*
2020	August, September, October, November

The wildfire records provided by fire agencies allow for the identification and quantification of historical wildfires, but they have limitations in terms of their spatial and temporal resolutions. Specifically, only fire perimeters are identified, without details on the shape of the burn areas. Also, they provide only the start and end dates of the fires and lack information on how the wild intensity evolves over time. To address these limitations, we used the solar irradiance data from the NSRDB as an indirect measure for the location and intensity of historical wildfires, given that the AOD caused by wildfire smoke directly affects the solar irradiance.

4.1.3 Market Data

CAISO's Open-Access Same-time Information System (OASIS) database provides access to all the market-relevant historical data necessary for this study. Within this database, five types of data have been identified as significant for this analysis. Table 6

summarizes their properties from the perspectives of data type, data source, spatial precision, temporal precision, and magnitude measure/unit.

Table 6. Market-Relevant Data Sets

Data Type	Data Source	Spatial Precision	Temporal Precision	Magnitude Measure/Unit
Real-time PV generation	CAISO OASIS	System level	5 min	MW
Real-time operating reserve		System level	5 min	MW
Day-ahead reserve requirement		Zone level	1 hour	MW
Energy locational marginal price (LMP)		Node level	1 hour (day ahead) 5 min (real time)	$/MW

The market data encompass different spatial resolutions, ranging from the system level to the zone level, to the node level. They are available in two distinct time frames: day ahead and real time. The day-ahead market data are provided at an hourly precision, whereas the real-time market data offer a higher level of granularity, with 5-minute precision.

4.2 Impact Analysis

4.2.1 Impact on PV Generation

The impacts of wildfire activity on solar generation are quantified at a monthly resolution and the system level using the wildfire record data and CAISO OASIS data. Figure 20 illustrates the monthly solar generation (blue areas) and curtailment (orange areas), which sum to the monthly net solar generation, as well as their relationships with respect to the rescaled 2019 baselines (green lines). The purple dashed lines show the months with burn areas exceeding 0.2 million acres. Note that 2019 was selected as the baseline year because it is the smallest fire year among the four. The rescaled baselines were created by scaling up/down the actual 2019 PV generation to match the peak generation in each year to diminish the influence of varying PV installation capacity. The blue bars on the bottom of the subfigures indicate the difference between the net PV generation and its rescaled 2019 baseline in each month. According to Figure 20, three observations can be made:

- Up to 10% monthly PV reductions are observed.
- Across the four years, the differences between the actual PV generation and the 2019 baselines are the most significant in 2020.
- Within each year, the largest negative differences are associated with months with burn areas exceeding 0.2 million acres.

Both observations indicate the impact of wildfire on suppressing PV generation. We made monthly instead of daily comparisons because we assumed that the monthly wildfire-free

PV generation profiles remained relatively constant across years, whereas that was not the case for the daily wildfire-free PV generation profiles.

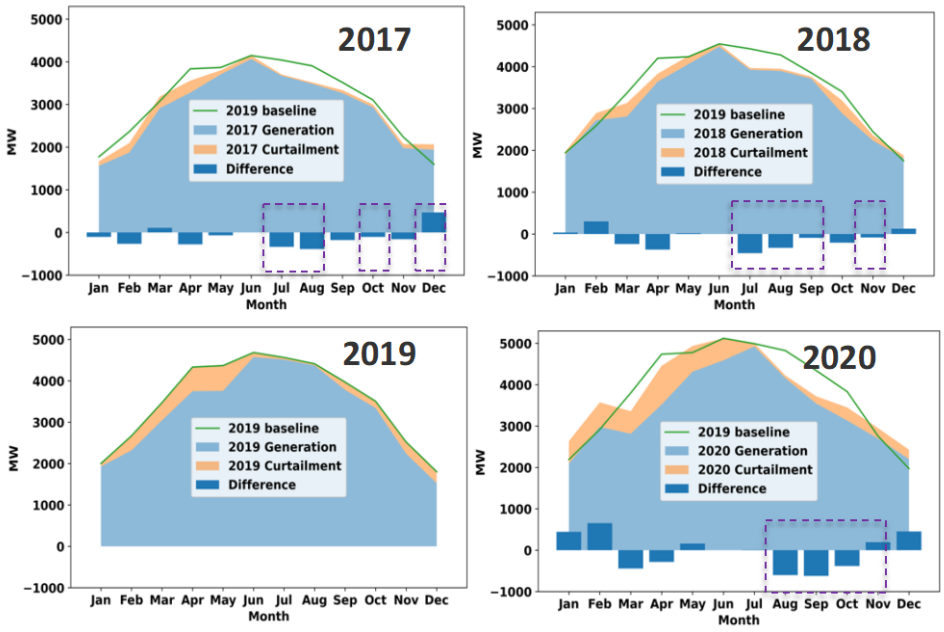

Figure 20. Monthly solar generation profiles. Purple dashed lines highlight the months with burn areas greater than 0.2 million acres.

4.2.2 Impact on Operating Reserve

Similar system-level monthly comparisons were made between the wildfire activity and the operating reserve. Figure 21 illustrates the monthly day-ahead minimum operating reserve requirement and the monthly real-time available operating reserve for the same 4 years from 2017–2020. The green bars on the bottom of the subfigures calculate the gaps between the real-time operating reserves and the day-ahead reserve requirements.

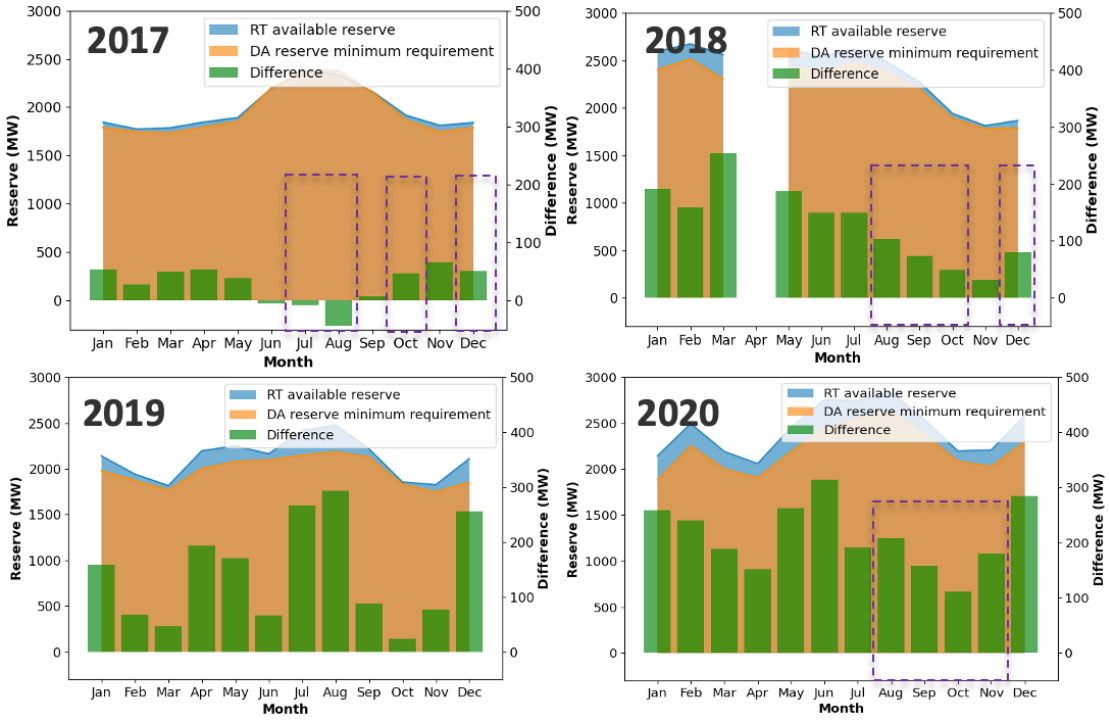

Figure 21. Monthly operating reserve profiles. Purple dashed lines highlight the months with burn areas greater than 0.2 million acres.

According to Figure 21, several observations can be made:

- Across the four years, 2020 and 2019 had the highest and lowest demand for system reserves.
- Within each year, months with burn areas exceeding 0.2 million acres had on average 50% less operating reserve surplus than other months.

Both observations indicate that wildfires could increase pressure on system operation by increasing the day-ahead reserve requirement and reducing the real-time available operating reserve surplus.

4.2.3 Impact on Market Price

We conducted a correlation analysis between wildfires and prices at both the system level and the zone level considering the higher spatial resolution of price data compared to PV generation and reserve data. Although price information is available at the node level, wildfire impact is typically regional due to smoke dispersion. As shown in Figure 14, in our study, we partitioned the California region into eight zones: Northern California, Bay Area, Northern Central Valley, Southern Central Valley, Los Angles, Eastern California, Southern California, and Central Coast.

Figure 22 shows the wildfire-price impact at the system level. It plots the ratios between the monthly averaged market price and the yearly averaged market price for 2017–2020. Table 7 summarizes the months when the monthly averaged market price exceeded the yearly average market price. The years 2017, 2018, and 2020 (years with greater burned areas) experienced increases in prices in the second half of the years, which coincided

with periods of greater wildfire influences; however, the year 2019 (the year with less burn areas) is an exception. In addition, Table 7 indicates that months with higher market prices highly overlap with months with greater wildfire burn areas. Specifically, 11 of 12 months with burn areas exceeding 0.2 million acres, highlighted in bold in Table 7, contributed to higher-than-average market prices.

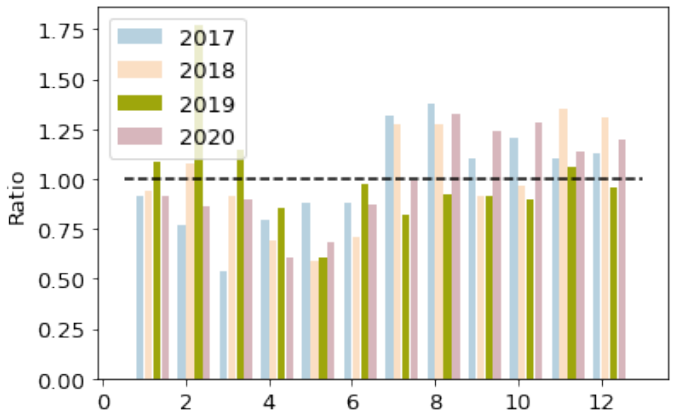

Figure 22. Ratios between monthly and yearly averaged prices. The black dashed line indicates where the monthly averaged price meets the yearly averaged price.

Table 7. Months With Higher-Than-Average Market Prices

Year	Months With Burn Areas Exceeding 0.2 Millions Acres
2017	**July**, **August**, November, **December**
2018	**July**, **August**, **September**, October, **November**, December
2019	January, February, March, November
2020	**August**, **September**, **October**, **November**, December

The monthly system-level analysis presented here provides limited information given the low data resolution. To leverage the market price data available at higher spatial and temporal resolutions, we further designed a wildfire-price correlation analysis based on the meteorological data provided by the NSRDB. Specifically, we calculated the differences between the clear-sky GHI, which represents the total amount of solar radiation received on a horizontal surface under cloud-free conditions, of the wildfire and no wildfire scenarios to represent the wildfire intensity in different areas, as given in Eq. (1).

$$WI = GHI_{clearsky}^{wildfire} - GHI_{clearsky}^{nowildfire} \quad (1)$$

Figure 23 presents a comparison between the daily total burn area profile, estimated by assuming an evenly distributed burn area between the start and end dates of the wildfire record, and the daily average wildfire index profile, calculated using the clear-sky GHI, across the 3 months. The two profiles exhibit similar patterns, with the highest values of both the wildfire index and burn area observed from August 15, 2020, to

September 15, 2020, followed by the median values observed after September 15, 2020, and the lowest values being observed before August 15, 2020.

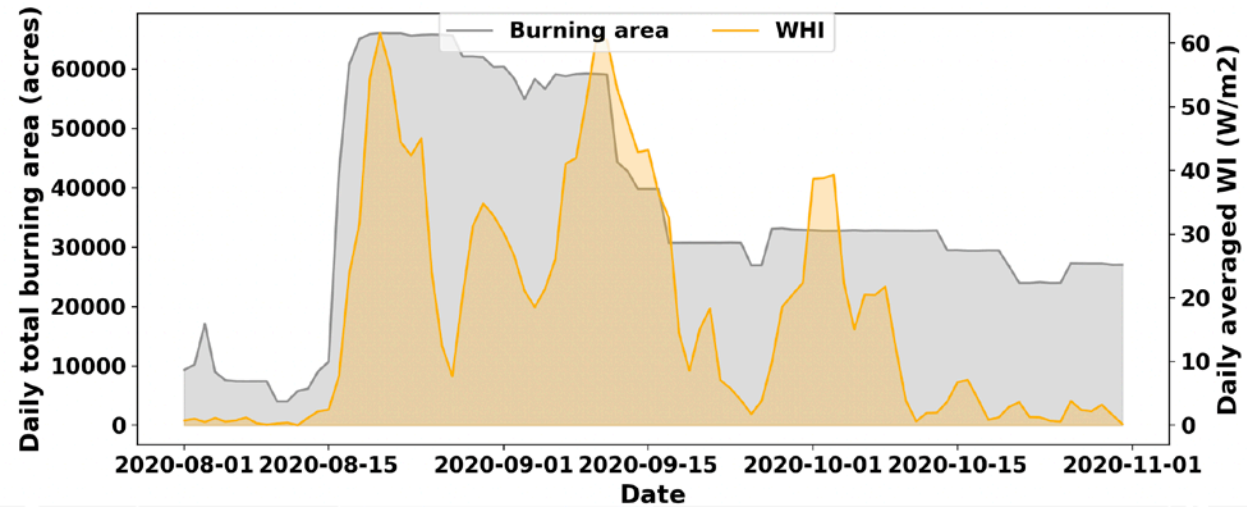

Figure 23. Daily total burn area versus daily averaged wildfire index

Figure 23 illustrates the correlation coefficients between the wildfire index and the market price for the 3 months with the highest wildfire impact in 2022. Three different approaches were applied to process the data:

1. Hourly averages: Averaged GHI differences (across each zone and at the hourly resolution) were calculated to quantify the wildfire intensity.
2. Daily averages: Averaged GHI differences (across each zone and at the daily resolution) were calculated to quantify the wildfire intensity.
3. Normalized hourly averages: The GHI were divided by the cosine value of the solar zenith angle to remove the impact of solar zenith angle before calculating the hourly averaged GHI difference.
4. Normalized daily averages: The GHI were divided by the cosine value of the solar zenith angle to remove the impact of solar zenith angle before calculating the daily averaged GHI difference.

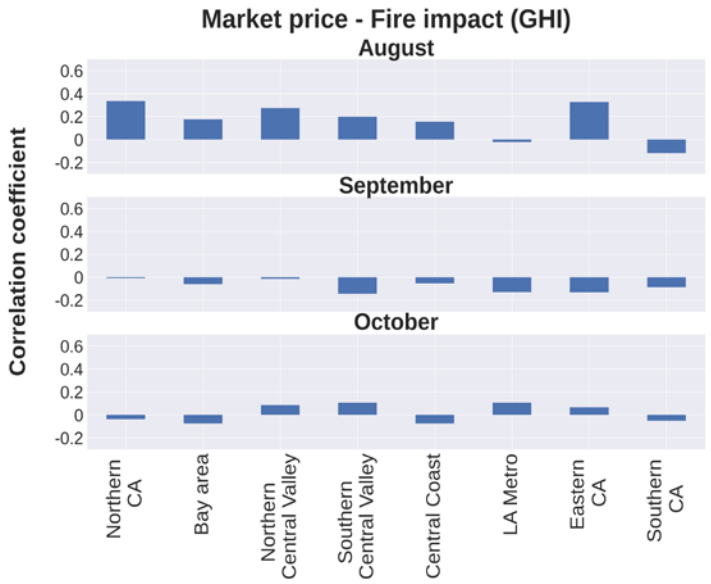

(a) Hourly average

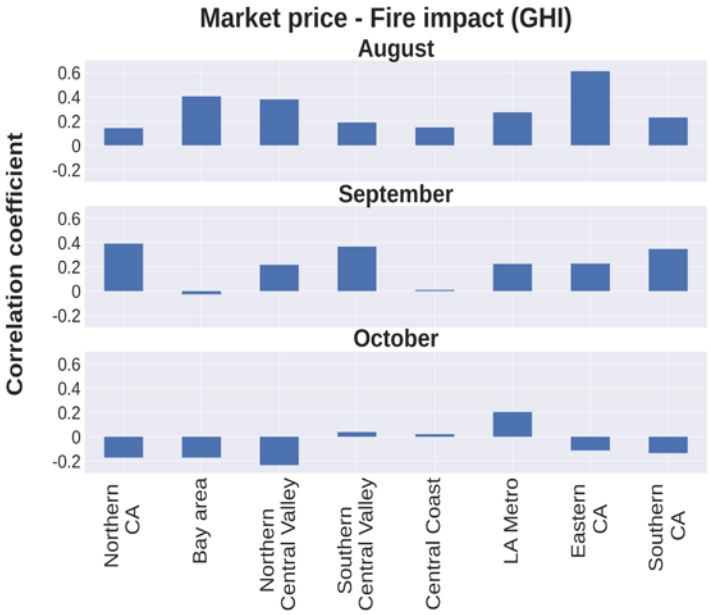

(b) Daily average

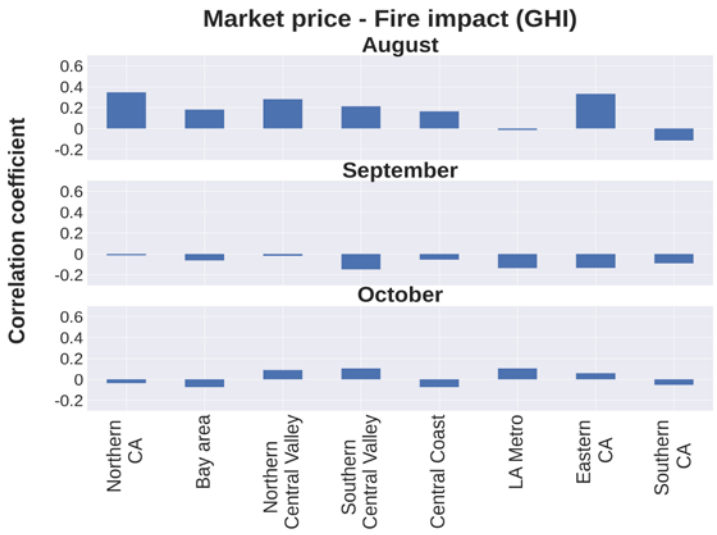

(c) Normalized hourly average

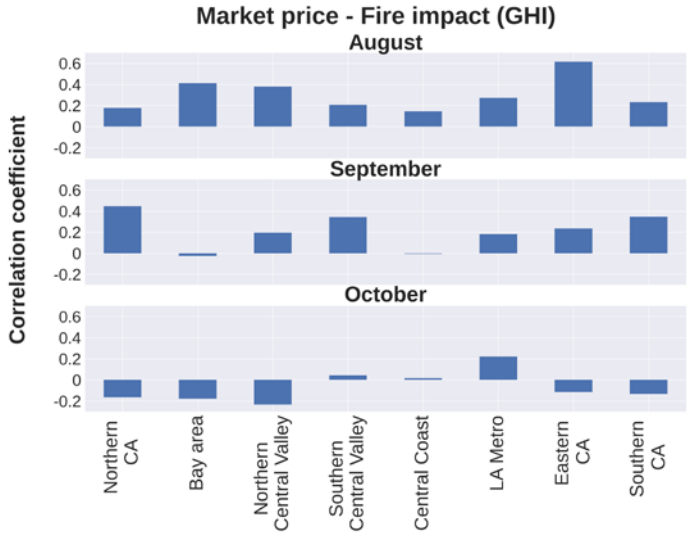

(d) Normalized daily average

Figure 24. Pearson correlations between the wildfire index and market prices in different zones

Figure 24 shows that there is a correlation between wildfires and market price at the zone level, especially during August. Because the system relies less on solar generation from August to October (with 25.95%, 23.33%, and 22.60% of the load served by solar generation in August, September, and October 2020, respectively), these correlations gradually decrease. During the month with the most significant correlation (August), higher correlation coefficients are found in zones with greater solar capacity, namely, the Southern Central Valley, the Los Angeles metropolitan area, and the Eastern California. When comparing different approaches for processing the data, note that stronger correlations are present when daily averages are compared. This is because the hourly averages of clear-sky GHI combine the influence of the time of the day, thereby not eliminating its impact on solar irradiation. In addition to that, normalization of the solar

irradiance based on solar angle does not have a significant impact on the wildfire-price correlation.

4.3 Limitations of Real-World Data Mining

Several challenges arise when conducting a wildfire-market price impact analysis solely based on real-world data:

1. The available wildfire records offer limited insight into the wildfire's market impact due to their low spatial and temporal resolutions, restricting our ability to examine the wildfire-market price impact at a high resolution.
2. Isolating the specific impact of wildfires on market prices using real-world data is a significant challenge because wildfire impact is only one of many operational factors that influence market prices. Unless data sets encompassing all relevant influencers—such as transmission contingency, generation outage, and load forecast—are identified and accessible, it would be highly challenging to discern the portion of market price variation solely attributed to wildfires.

5 Market Impact Analysis: PLEXOS Simulation

Due to the limitations associated with real-world data mining, as discussed in Section 4.3, we conducted additional market impact analysis using PLEXOS. This approach offers several advantages:

1. Simulation data can be obtained at flexible spatial and temporal resolutions, which can enable more detailed examinations of the impact analysis.
2. Simulations provide the opportunity to control and compare other influential factors, allowing researchers to isolate and evaluate the specific influence of wildfires on various market variables.
3. By using configurable system models and inputs, researchers can effectively investigate the effects of increasing occurrences and intensities of wildfires and their effects on PV penetration on the market, uncovering future trends. Such a futuristic analysis serves as valuable information for policymakers, businesses, and stakeholders, facilitating the development of strategies to mitigate risks, enhance resilience, and optimize decision-making processes.

5.1 Data Preparation

Using the widely adopted PLEXOS software, the developed simulation model encompasses the entire Western Electricity Coordinating Council (WECC) region. In this section, we present comprehensive information regarding the inputs that were incorporated into the model, which encompass various aspects such as power sector infrastructure, renewable generation profiles, demand profiles, and reserve requirements.

5.1.1 Power Sector Infrastructure

Figure 25 illustrates the process taken for generating the PV metadata using three NREL in-house software tools: the Regional Energy Deployment System (ReEDS™), the Renewable Energy Potential (reV) model, and the Distributed Generation Market Demand (dGen™) model. Initially, ReEDS makes electricity sector investment decisions based on system and unit constraints and the projected energy and ancillary service demands at the balancing authority level. Specifically, the least-cost resource mix, the locations for the thermal and renewable resource deployment, as well as the transmission infrastructure expansion to accommodate those installations are generated as the outputs, based on which reV is further applied to translate the building authority-level capacities into nodal capacities given specific generator locations. dGen, on the other hand, is used to simulate customer adoption of distributed rooftop solar panels considering the technical, financial, and geographic factors that drive the market potential.

Both ReEDS and dGen provide a variety of scenarios that reflect the diverse assumptions made in technology cost, thermal generator retirements, policy regulations, demand growth, and vehicle electrification. Table 8 summarizes the assumptions made in our study for creating the two power sector infrastructure plans. Note that we selected two power sector infrastructures to represent different levels of renewable penetration: the infrastructure years 2024 and 2036 with solar penetration levels of 32% and 36%,

respectively. Figure 26 shows the modeled PV locations and capacities for both infrastructure plans in the California region.

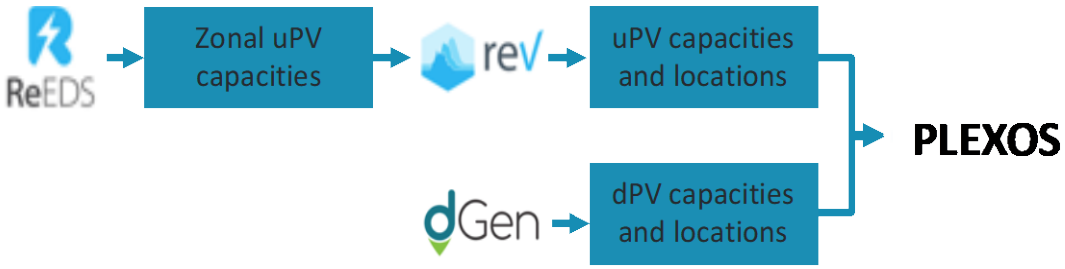

Figure 25. Steps for creating the PV metadata

Table 8. Assumptions for Each Power Sector Infrastructure Plan

Infrastructure Year	Generator Cost and Performance Assumption	Renewable Energy Resource Supply Curves	Distributed Generation Assumptions	Solar Penetration Levels in California
2024	2019 ATB Mid-Case (Cole et al. 2019)	2019 Standard Scenarios Mid-Case (Vimmerstedt et al. 2019)	dGen Mid-Cost RE adoption (Sigrin et al. 2016)	32%
2036	2019 ATB Low for PV and Wind (Cole et al. 2019)		dGen Low-Cost RE adoption (Sigrin et al. 2016)	36%

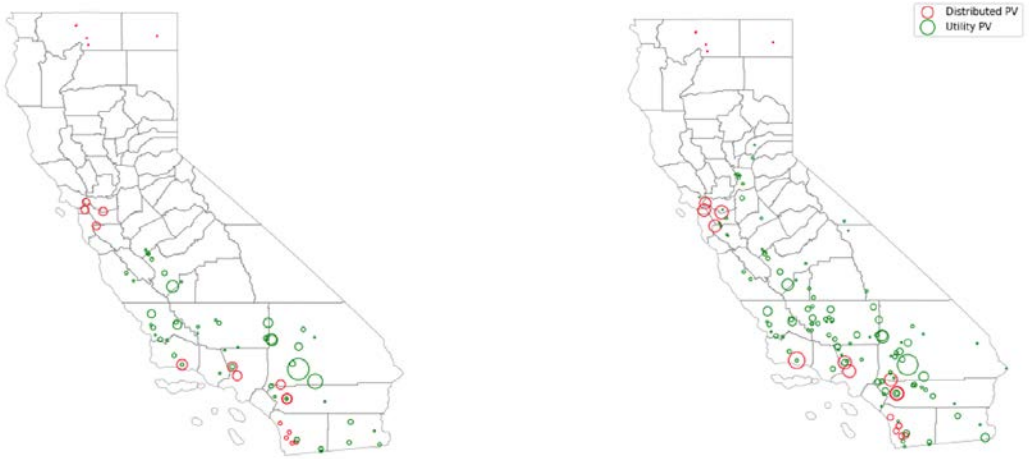

Infrastructure year 2024 Infrastructure year 2036

Figure 26. Distributions of utility-scale PV and distributed PV capacities for two infrastructure years. Size of the circles represent nameplate capacity

5.1.2 Renewable Generation Profiles

Using the power sector infrastructure plans and AOD profiles produced for different wildfire scenarios (explained in Section 2), we generated time-series data for PV generation. These data encompass the no wildfire scenario, the 2020 wildfire scenario,

and the enhanced wildfire scenario spanning two infrastructure years. To accomplish this, we used the System Advisor Model (SAM), a techno-economic renewable adaption model developed at NREL. SAM allowed us to create comprehensive PV generation profiles for both utility-scale and distributed PV plants at the nodal level considering the plants' locations and capacity metadata. Note that because the AOD scenarios are generated covering the California region only, the PLEXOS model was created for the whole WECC footprint. For utility-scale and distributed PV located outside California, NSRDB 2020 observed data were applied to create the PV generation profiles, and they remained the same for all six wildfire scenarios.

For the wind generation profiles, we remain use wind profiles from the existing project[4] that generated based on 2012's weather data, given that wildfire's impact on wind generations is not the focus of this study.

5.1.3 Demand Profiles

To capture the correlations between load and renewable generation driven by the underlying weather time-series pattern in 2020, we collected building authority-level 2020 load profiles from the WECC Anchor Dataset (ADS) and applied load projection factors from the U.S. Energy Information Administration Annual Energy Outlook data set to scale up the loads to reflect the demand growth in infrastructure years 2024 and 2036.

5.1.4 Reserve Requirements

Operating reserves are critical for maintaining balance between the system supply and demand and for restoring system stability after disturbances. Operating reserves are either self-scheduled or competitively procured by CAISO from qualified scheduling coordinators in the day-ahead and real-time markets. CAISO determines the reserve requirement to meet the North American Electric Reliability Corporation and WECC reliability standards, which are traditionally calculated as percentages of the applicable CAISO forecast of CAISO demand for the day-ahead and real-time markets at the regional level. With increasing integrations of renewable generation, which introduce considerable amounts of variabilities and uncertainties, a new operating requirement is proposed that relies on not only the load forecast but also the renewable forecast. In our study, we simulated only the real-time market; therefore, the operating reserve requirement was designed to address only the real-time variability and uncertainty. We followed the approach proposed in an existing study and calculated the regional-level reserve requirements based on PV forecasting errors associated with hourly PV forecasting.

In the developed production cost model, regional-level reserve requirements are defined to cover the uncertainty (forecasting error) in wind and solar generation (Ibanez et al. 2013). Such requirements are determined based on sub-hourly variability of the PV and wind generation. For the wind reserve requirement, because the short-term variability of wind is low, a persistence forecast is applied to predict the wind generation and analyze the wind forecasting errors. For the PV reserve requirement, because the variability of PV

can be modeled by the clear-sky GHI, a Solar Power Index (SPI) persistence forecast is applied to predict the PV generation and to analyze the PV forecasting errors. The regulation reserve requirements are based on 10-minute persistence forecasts and confidence intervals that cover 95% of the forecast errors. The total operating reserve requirement that jointly considers uncertainties in load, PV, and wind can then be calculated as:

$$RR_{total} = \sqrt{(1\%Load)^2 + (RR_{wind})^2 + (RR_{PV})^2} \quad (2)$$

where RR_{wind} and RR_{PV} represent the reserves required by wind and PV, and $Load$ is the system-level load.

Note that only regulation-up reserves (caused by down ramps from wind/PV) were simulated in this study because we assumed that excessive energy from wind and PV could be curtailed if there was a need for regulation down.

5.1.5 Clear-Sky GHI Profiles

Because we analyzed only the wildfire impact to solar irradiance in this study, differences between clear-sky GHI in a wildfire scenario (i.e., 2020 wildfire or enhanced wildfire) and a no wildfire scenario were applied to quantify the intensity of wildfires, the same as the wildfire indexes introduced in Eq. (1) in Section 4.

5.2 Impact Analysis

5.2.1 Impact on PV Generation

The dotted line plots in Figure 27 compare the monthly PV generation profiles created based on the AOD conditions under the three wildfire scenarios with PV plant metadata (i.e., location and capacity) for two infrastructure years. The bar plots on the bottom indicate the PV generation drop given the 2020 wildfire and enhanced wildfire scenarios.

Figure 27 displays dotted line plots that compare the monthly PV generation profiles generated using AOD profiles for three wildfire scenarios with PV plant metadata (i.e., location and capacity) for two infrastructure years. The bar plots at the bottom of the figure depict the extent of PV generation reduction caused by the 2020 wildfire and enhanced wildfire scenarios. Specific values of the PV generation decreases are shown in Table 9 and Table 10.

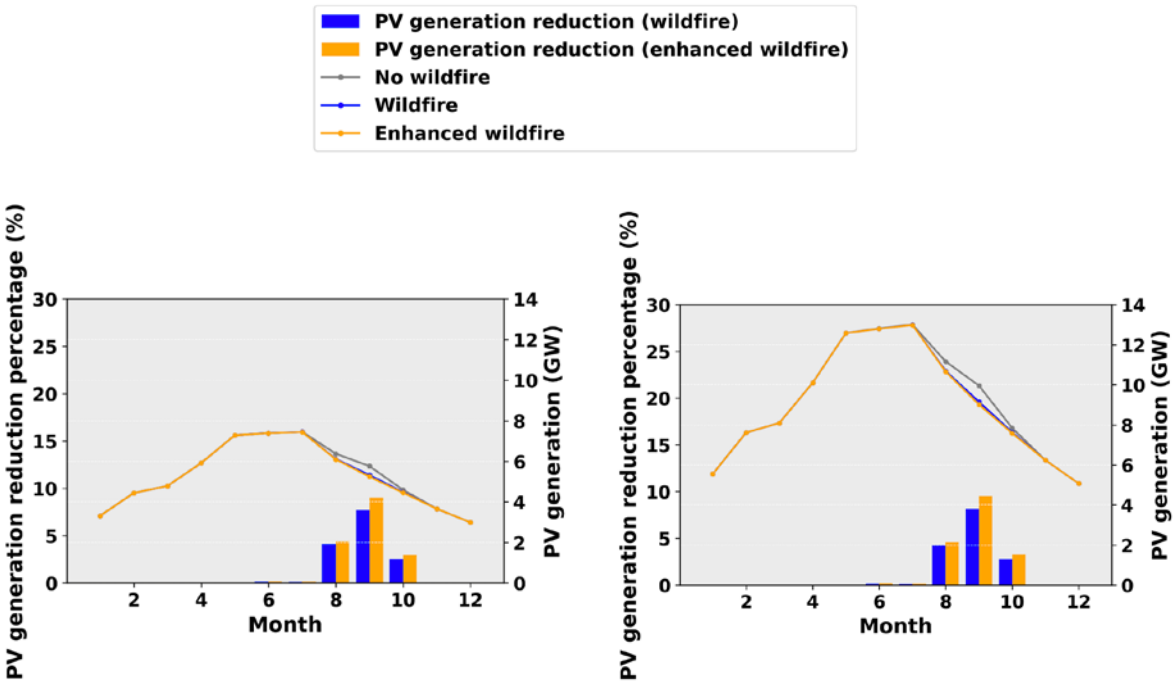

(a) Infrastructure year 2024

(b) Infrastructure year 2036

Figure 27. Average hourly PV generation profiles for two infrastructure years

Table 9. Average Hourly PV Generation Reductions for Infrastructure Year 2024

Scenario	Reduction in generation (MW)				
	June	July	August	September	October
2020 Wildfire	10.8	7.8	263.2	443.9	115.1
Enhanced Wildfire	12.2	10.3	280.1	519.9	136.8

Table 10. Average Hourly PV Generation Reductions for Infrastructure Year 2036

Scenario	Reduction in generation (MW)				
	June	July	August	September	October
2020 Wildfire	18.6	12.6	477.9	809.1	216.9
Enhanced Wildfire	21.4	17.0	510.7	947.7	257.5

The outcome indicates that the 2020 wildfires resulted in a decrease of up to 7.7% in monthly PV generation, with September experiencing the most significant reduction. Additional reductions of 0.4% and 1.3% were attributed to the enhanced wildfire and increased PV deployment scenarios, respectively.

5.2.2 Impact on Operating Reserve

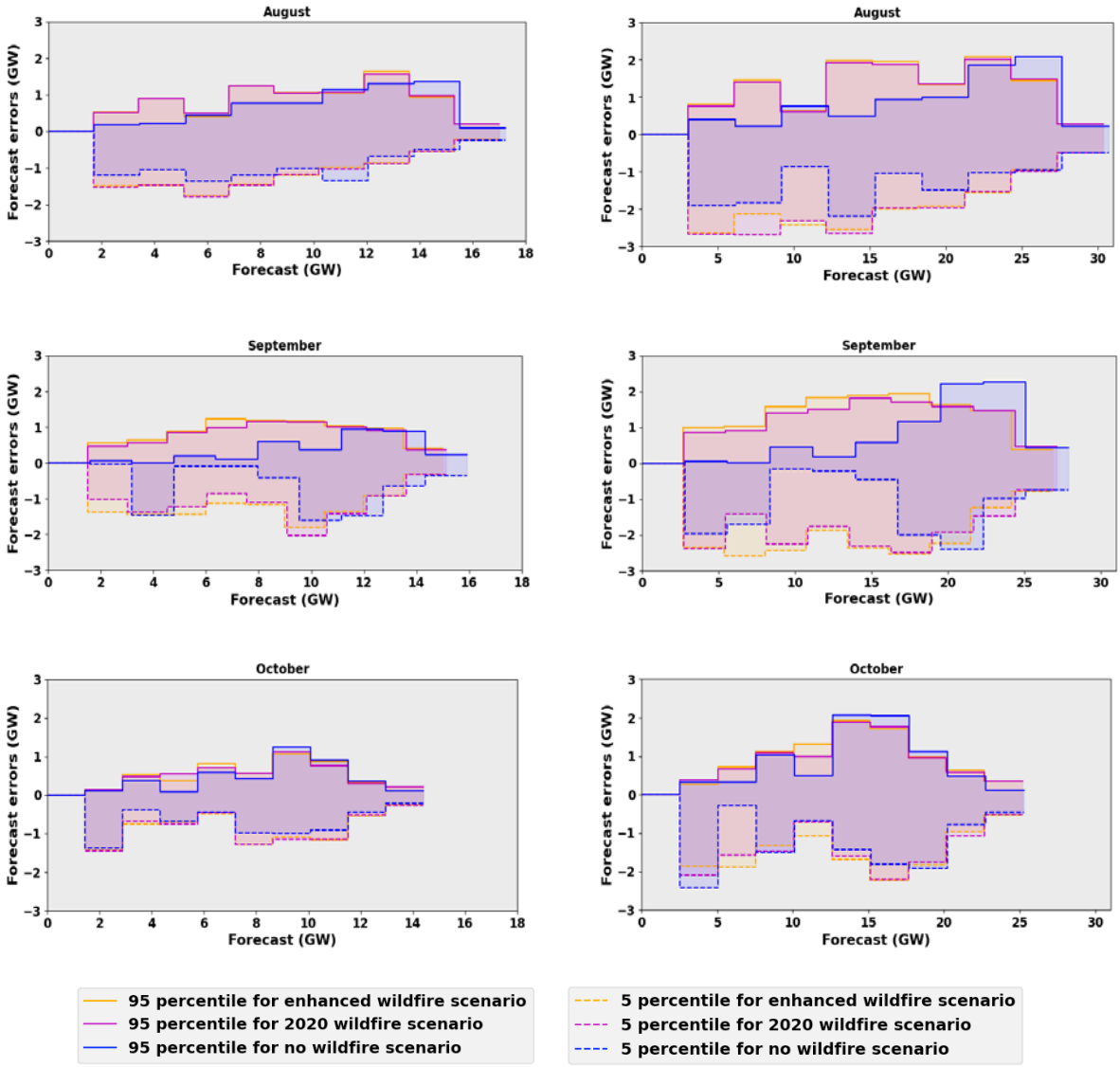

(a) Infrastructure year 2024

(b) Infrastructure year 2036

Figure 28. Percentiles (95% and 5%) for system PV forecasting errors for two infrastructure years

The area plots in Figure 28 compare the 90% confidence intervals of the solar forecasting errors across three wildfire scenarios in two infrastructure years. The dashed and solid lines indicate the 5th and 95th percentiles, respectively. We found that wider confidence intervals are observed as the wildfire becomes more severe, indicating higher uncertainty. Although there is a significant difference between the scenarios without wildfire and those with the 2020 wildfire, the disparity is relatively small when comparing the enhanced wildfire scenario to the 2020 wildfire scenario.

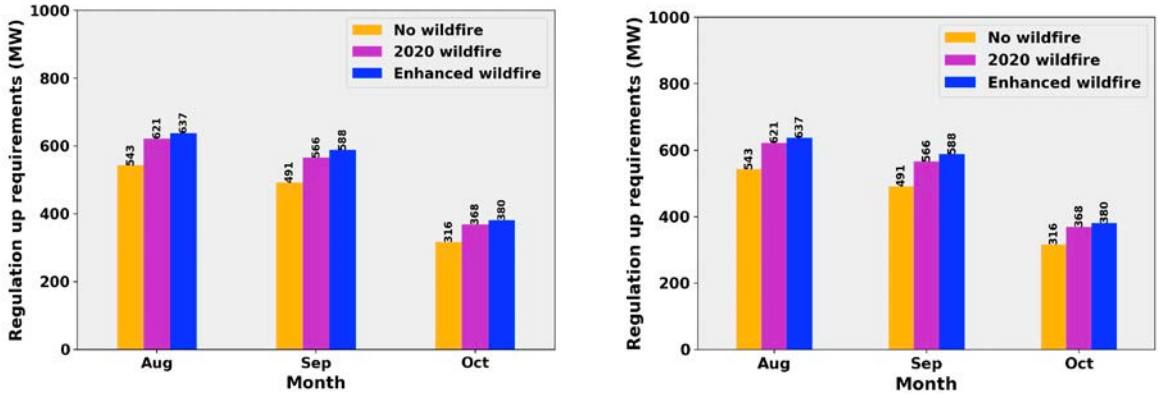

(a) 2024 (b) 2024

Figure 29. Monthly averaged reserve requirement

Using the 95th percentile as the standard for the regulation-up requirement, we computed the average regulation-up requirement across three wildfire scenarios in two infrastructure years. These results are visualized in the bar plots in Figure 29. Despite the relatively small effects of wildfire on PV generation (8%–9% reduction), we observed more substantial impacts on the PV reserve requirements. Specifically, the 2020 wildfire and enhanced wildfire scenarios lead to an increase in the monthly PV reserve requirements by as much as 53% and 64%, respectively.

5.2.3 Impact on Market Price

Table 11 and Table 12 provide a summary of market price statistics, including the mean, standard deviation, and the percentage of time when the market price exceeded $100/MW (P [price > $100/MW]). These statistics are presented for three wildfire scenarios in two infrastructure years. The findings indicate that wildfires could potentially increase the market price, on average, while introducing more price volatility and price spikes. A more pronounced effect is observed on increasing the variability of prices rather than increasing the average price.

Table 11. Market Price Statistics for Infrastructure Year 2024

Statistic	Scenario		
	No Wildfire	2020 Wildfire	Enhanced Wildfire
Mean	39.27 $/MW	39.57 $/MW	39.62 $/MW
Standard deviation	17.20 $/MW	20.57 $/MW	22.15 $/MW
P [price > $100/MW]	0.16%	0.19%	0.20%

Table 12. Market Price Statistics for Infrastructure Year 2036

Statistic	Scenario		
	No Wildfire	2020 Wildfire	Enhanced Wildfire
Mean	72.83 $/MW	75.80 $/MW	76.17 $/MW
Standard deviation	256.07 $/MW	263.50 $/MW	264.94 $/MW
P [price > $100/MW]	5.59%	5.82%	5.82%

In addition, we examined the impact of wildfire location on market price. To achieve this, two wildfire indexes were introduced to quantify the system-wide wildfire impact, and comparing the differences between them allowed us to gauge variations in wildfire distribution. These indexes were the averaged wildfire intensity and the weighted wildfire intensity. The averaged wildfire intensity, as given in Eq. (3), is calculated by taking the simple average of the clear-sky GHI differences between two wildfire scenarios across all transmission nodes. The weighted wildfire intensity, as given in Eq. (4), is determined by taking the weighted average of the GHI differences based on the PV installation capacity at each transmission node.

$$Averaged\ wildfire\ intensity = \frac{\sum_{n\in N}(clearsky\_GHI_n^{nowildfire} - clearsky\_GHI_n^{2020wildfire})}{|N|} \quad (3)$$

$$Weighted\ wildfire\ intensity = \frac{\sum_{n\in N}(clearsky\_GHI_n^{nowildfire} - clearsky\_GHI_n^{2020wildfire})\cdot C_n}{\sum_{n\in N} C_n} \quad (4)$$

The three plots in the lower section of Figure 30 illustrate the wildfire intensity, energy price, and load variations under the three wildfire scenarios in infrastructure year 2024. The blue and pink areas represent the comparison of day-to-day averaged and weighted variations in wildfire intensity. The dotted gray and orange curves represent the daily averaged prices for the no wildfire and 2020 wildfire scenarios, respectively. Additionally, the gray area plots capture the system-level load variation along with the price and wildfire intensity.

To understand how the location of wildfires, with respect to the PV installation capacity distribution, influences the market price, we selected two days that had comparable system loads and averaged wildfire intensities but different weighted wildfire intensities, as indicated by the green and purple frames. In the upper section of Figure 30, a price change and a wildfire map are plotted for each day to display the geographic distributions of the price changes and the wildfire intensities under the 2020 wildfire scenario. A comparison of the two wildfire maps reveals that the day with a relatively lower weighted wildfire intensity experienced more intense wildfires in Northern California, whereas the

day with a relatively higher weighted wildfire intensity experienced wildfires predominantly in the south, where there is a higher PV installation capacity. Moreover, comparing the two price change maps indicates that a more pronounced increase in price occurs when wildfires are in closer proximity to areas with dense PV installations.

Using the aforementioned wildfire intensity indexes, we conducted further analysis to quantify the correlations between wildfires and price at both the system level and node level. Table 13 presents a comparison of the Pearson correlations between the averaged prices and the averaged/weighted wildfire intensities considering daily resolution and system-level measurements. The results show that in the year 2036, with higher PV penetration, and when using the weighted wildfire intensity index, stronger correlations between wildfires and price are observed. Figure 31 depicts the distributions of wildfire-price correlations for the influence of the 2020 wildfires and enhanced wildfires in two infrastructure years. The figure indicates that as PV penetration increases, the influence of wildfires on price becomes more widespread. Note that the enhancement of wildfires does not affect the distributions of wildfire-price correlations.

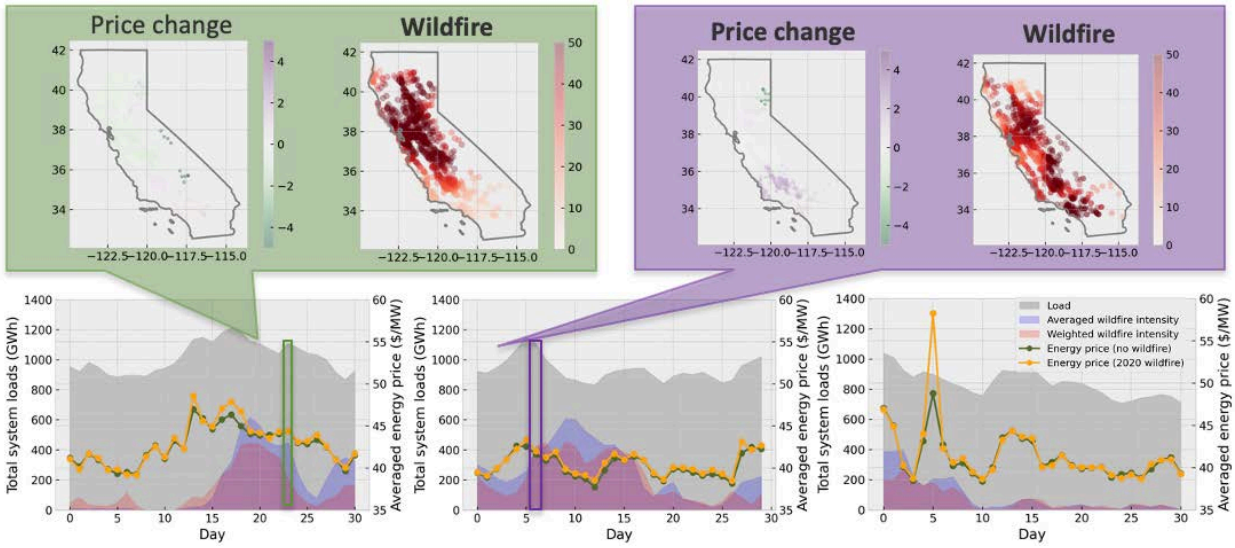

Figure 30. Wildfire intensity, energy price, and load variations under three wildfire scenarios in infrastructure year 2024

Table 13. System-Level Wildfire-Price Correlations Under Three Wildfire Scenarios in Two Infrastructure Years

R^2	Weighted Wildfire Intensity	Averaged Wildfire Intensity
2024 (2020 wildfire)	0.20	0.16
2024 (enhanced wildfire)	0.18	0.15
2036 (2020 wildfire)	0.40	0.35
2036 (enhanced wildfire)	0.46	0.39

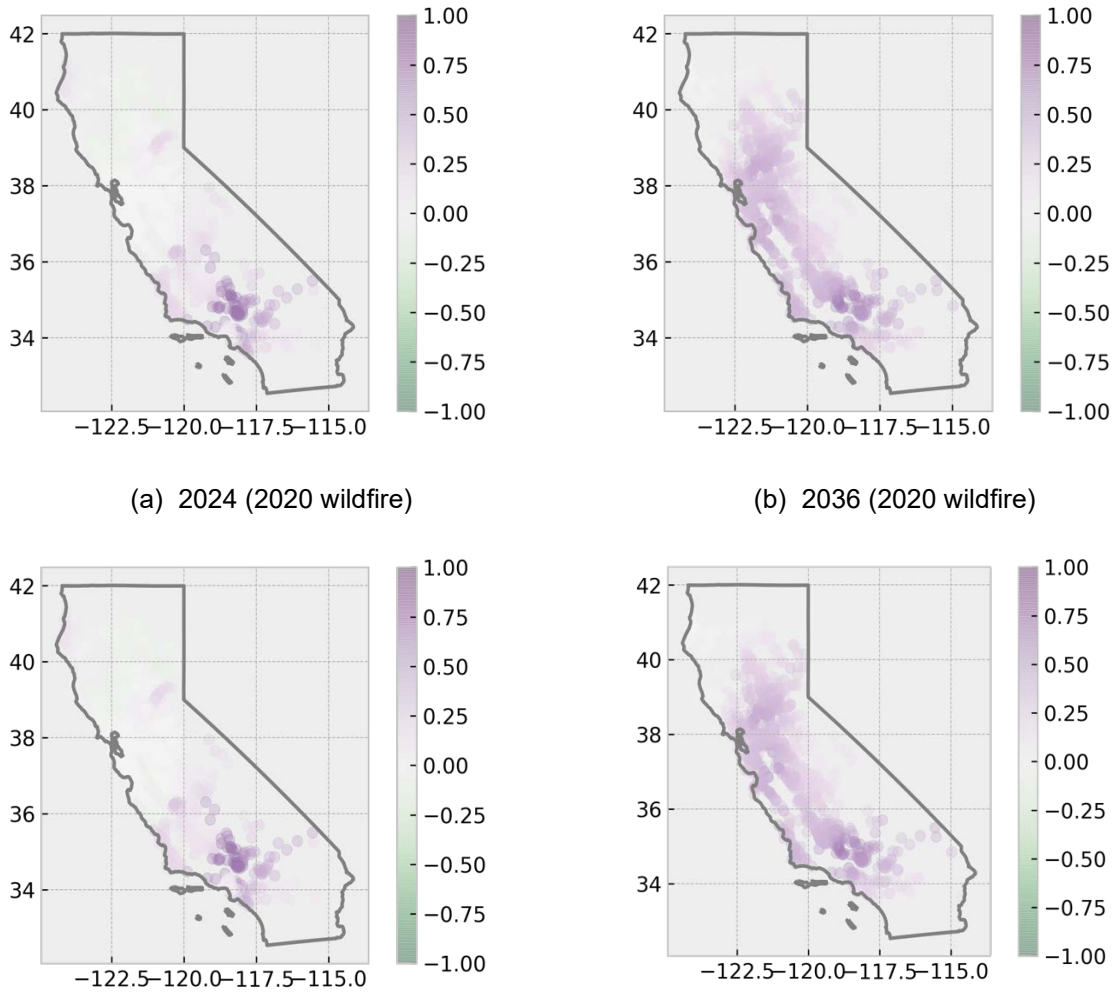

(a) 2024 (2020 wildfire)

(b) 2036 (2020 wildfire)

(c) 2024 (enhanced wildfire)

(d) 2036 (enhanced wildfire)

Figure 31. Node-level wildfire-price correlations

6 Conclusions and Future Work

Wildfire activity over North America has been observed to exhibit an increasing trend during the past decades and is projected to increase under a changing climate with warmer and drier conditions. Wildfires can emit considerable amounts of smoke aerosols in the atmosphere, which not only lead to air quality issues but also significantly reduce solar radiation. Sudden large reductions of the solar resource could affect solar generation and reserves, introducing uncertainties in power generation and market price and increasing the vulnerability of solar power plants. This effect is expected to become more important with increasing trends in wildfires and higher levels of solar deployment. Therefore, this project investigated and quantified wildfire-caused changes in atmospheric aerosol loading and thus on the solar resource, solar generation, reserve, and market price based on an analysis of historical data and numerical experiments. We conducted simulations of solar radiation using NREL's PSM and NSRDB, and of solar generation, reserve, and market price using PLEXOS under various wildfire scenarios (background AOD, 2020 wildfire, and enhanced wildfire) and two solar penetration scenarios (based on projected penetration in 2024 and 2036).

For the development of the AOD and solar radiation data sets, an evaluation of the NSRDB and PSM showed that the NSRDB can well capture both the AOD and solar radiation during the high fire activity period in 2020. This indicates that using the PSM and the NSRDB is an appropriate approach to study wildfire impacts on the solar resource. To quantify the wildfire impacts, comparisons between the 2020 wildfire and background AOD scenarios showed that the monthly AOD increased by 0.14–0.46 (140%-460%) in the 2020 wildfire scenario, where the background AOD is approximately 0.10. The enhanced AOD levels lead to a reduction in monthly GHI and DNI by approximately 3%–7% and 9%–23%, respectively, during August–October 2020. Accounting for the projected increase in the burn areas in California, simulations suggested increases in the monthly AOD over California and more moderate decreases in the monthly clear-sky DNI. Given the limited scope of our study, however, our analysis does not capture the full variability (wildfire location, size, time of year, aerosol indirect effects), which can be equally important. Further, the impact of enhanced fire activity on clear-sky DNI could be greater on shorter (daily) timescales, and the impacts can significantly vary by region.

According to our wildfire-market price analysis, the 2020 wildfires resulted in monthly reductions of up to 5% in PV generation and an increase of 53% in monthly operating reserve requirements. With escalating wildfire activity, these numbers could potentially increase to reductions of up to 6% in PV generation and an increase of up to 64% in the operating reserve requirement. Compared to the average GHI differences, weighted GHI differences proved to be a better indicator for assessing the system-level impacts of wildfires on market price. Generally, nodes with higher PV installation capacities demonstrate a greater impact on the correlation between wildfires and price than nodes in closer proximity to the wildfire centroid. As the trend of increasing PV deployment continues, it is expected that the wildfire impacts on market price will become more severe and widespread. Beyond the 2020 wildfire scenario, no significant additional market impact resulting from the modeled wildfire enhancement has been observed. This finding

suggests that the severity of the 2020 wildfire alone is substantial enough, indicating that 2020 could serve as a valuable fire year to be further investigated.

For future work, there are several avenues for improving the analysis conducted here. The wildfire scenarios were focused on fires in California alone, although wildfire smoke effects on AOD can occur at large downwind distances. Additionally, future fire scenarios ("enhanced fire" scenario of this study) can be made more realistic by accounting for simulated impacts of climate change, which were not included here due to limited scope of this analysis. Similarly, power sector analysis can also be improved. First, incorporating more realistic profiles for other sectors—such as wind, thermal outages, and hydropower—would provide a more comprehensive understanding of the system dynamics. Currently, our production cost model (PLEXOS) supports only real-time simulations, neglecting day-ahead scheduling and load, solar, and wind forecasts. To address this limitation, an extension of the production cost model to enable day-ahead/real-time simulations could be developed. This would involve creating day-ahead forecasts for load, wind, and solar, allowing for an analysis of the impact of day-ahead forecasting errors on market operation under various wildfire scenarios. Additionally, investigating the potential benefits of different designs of operating reserve requirements in mitigating the risks introduced by wildfires could be an intriguing research topic. This analysis could focus on examining how varying reserve requirements can help reduce real-time risks, such as price spikes and reserve shortages resulting from wildfires. Such an investigation would provide valuable insights into optimizing reserve strategies to enhance system reliability and resilience in the face of wildfire-induced challenges. Moreover, although the western United States is where most fires occur, the atmospheric transport of smoke can also affect other parts of the country, as seen in the summer of 2023 with the fires in Canada significantly affecting the air quality and AOD in parts of eastern United States.[12] Future analysis can be more comprehensive by including all of North America to understand the impacts in a scenario with simultaneous fires in several regions. This analysis focused on only California, but the fire impact on solar generation and the subsequent impact is likely to be observed in other regions of the United States as well as outside the United States (including Europe, Southeast Asia, and Australia) where large fires recurrence has been becoming more frequent.

[12] See "Smoke Causes U.S. Solar Power Generation To Plunge By 50%": https://oilprice.com/Alternative-Energy/Solar-Energy/Smoke-Causes-US-Solar-Power-Generation-To-Plunge-By-50.html. Accessed June 10, 2023.

References

Abatzoglou, J. T., and A. P. Williams. 2016. “Impact of Anthropogenic Climate Change on Wildfire Across Western U.S. Forests.” *Proceedings of the National Academy of the Sciences of the United States of America* 113: 11770–11775. https://doi.org/10.1073/pnas.1607171113.

Akdemir, K. Z., J. D. Kern, and J. Lamontagne. 2022. “Assessing Risks for New England’s Wholesale Electricity Market From Wind Power Losses During Extreme Winter Storms.” *Energy* 251. https://doi.org/10.1016/j.energy.2022.123886.

Balch, J. K., B. A. Bradley, J. T. Abatzoglou, R. Chelsea Nagy, E. J. Fusco, and A. L. Mahood. 2017. “Human-Started Wildfires Expand the Fire Niche Across the United States.” *Proceedings of the National Academy of Sciences of the United States of America* 114: 2946–2951. https://doi.org/10.1073/PNAS.1617394114/-/DCSUPPLEMENTAL/PNAS.201617394SI.PDF.

Barbero, R., J. T. Abatzoglou, N. K. Larkin, C. A. Kolden, and B. Stocks. 2015. “Climate Change Presents Increased Potential for Very Large Fires in the Contiguous United States.” *International Journal of Wildland Fire* 24: 892–899. https://doi.org/10.1071/WF15083.

Brown, T. J., B. L. Hall, and A. L. Westerling. 2004. “The Impact of Twenty-First Century Climate Change on Wildland Fire Danger in the Western United States: An Applications Perspective.” *Climate Change* 62: 365–388. https://doi.org/10.1023/B:CLIM.0000013680.07783.de.

California Department of Forestry and Fire Protection (CAL FIRE). 2023. “Statistics.” Our Impact. https://www.fire.ca.gov/stats-events/.

Chin, M., R. B. Rood, S.-J. Lin, J. F. Müller, and A. M. Thompson. 2000. “Atmospheric Sulfur Cycle Simulated in the Global Model GOCART: Model Description and Global Properties.” *Journal of Geophysical Research: Atmospheres* 105 (D20): 24671– 24687. https://doi.org/10.1029/2000JD900384 .

Chou, M.-D., and M. J. Suarez. 1999. *A Solar Radiation Parameterization for Atmospheric Studies*. Technical Report Series on Global Modeling and Data Assimilation. Greenbelt, MD: National Aeronautics and Space Administration. Tech. Rep. NASA/TM-1999-104606, Vol. 15. https://ntrs.nasa.gov/api/citations/19990060930/downloads/19990060930.pdf.

Cole, Wesley, Nathaniel Gates, Trieu Mai, Daniel Greer, and Paritosh Das. 2020. “2019 Standard Scenarios Report: A U.S. Electric Sector Outlook.” Presented on January 9, 2020. Golden, CO: National Renewable Energy Laboratory. NREL/PR-6A20-75798. https://www.nrel.gov/docs/fy20osti/75798.pdf.

Donaldson, D. L., D. M. Piper, and D. Jayaweera. 2021. "Temporal Solar Photovoltaic Generation Capacity Reduction from Wildfire Smoke." *IEEE Access* 9: 79841–79852. https://doi.org/10.1109/ACCESS.2021.3084528.

Dong, C., A. P. Williams, J. T. Abatzoglou, K. Lin, G. S. Okin, T. W. Gillespie, D. Long, Y.-Y. Lin, A. Hall, and G. M. MacDonald. 2022. "The Season for Large Fires in Southern California Is Projected to Lengthen in a Changing Climate." *Communications Earth and Environment* 3: 1–9. https://doi.org/10.1038/s43247-022-00344-6.

Emmons, L. K., S. Walters, P. G. Hess, J.-F. Lamarque, G. G. Pfister, D. Fillmore, C. Granier, A. Guenther, D. Kinnison, T. Laepple, J. Orlando, X. Tie, G. Tyndall, C. Wiedinmyer, S. L. Baughcum, and S. Kloster. 2010. "Description and Evaluation of the Model for Ozone and Related Chemical Tracers, Version 4 (MOZART-4)." Geoscientific Model Development 3: 43–67. https://doi.org/10.5194/gmd-3-43-2010.

Flannigan, M. D., M. A. Krawchuk, W. J. DeGroot, B. M. Wotton, and L. M. Gowman. 2009. "Implications of Changing Climate for Global Wildland Fire." *International Journal of Wildland Fire* 18: 483–507. https://doi.org/10.1071/WF08187.

Ford, B., M. Val Martin, S. E. Zelasky, E. V. Fischer, S. C. Anenberg, C. L. Heald, and J. R. Pierce. 2018. "Future Fire Impacts on Smoke Concentrations, Visibility, and Health in the Contiguous United States." *GeoHealth* 2: 229–247. https://doi.org/10.1029/2018gh000144.

Forrest, K., B. Tarroja, F. Chiang, A. AghaKouchak, and S. Samuelsen. 2018. "Assessing Climate Change Impacts on California Hydropower Generation and Ancillary Services Provision." *Climatic Change* 151 (3–4): 395–412. https://doi.org/10.1007/s10584-018-2329-5.

Gilletly, S. D., N. D. Jackson, and A. Staid. 2021. "Quantifying Wildfire-Induced Impacts to Photovoltaic Energy Production in the Western USA." *Proceedings of the IEEE Photovoltaic Specialists Conference*: 1619–1625. https://doi.org/10.1109/PVSC43889.2021.9518514.

Grell, G. A., and S. R. Freitas. 2014. "A Scale and Aerosol Aware Stochastic Convective Parameterization for Weather and Air Quality Modeling." *Atmospheric Chemistry and Physics* 14: 5233–5250. https://doi.org/10.5194/acp-14-5233-2014.

Guenther, A., T. Karl, P. Harley, C. Wiedinmyer, P. I. Palmer, and C. Geron. 2006. "Estimates of Global Terrestrial Isoprene Emissions Using MEGAN (Model of Emissions of Gases and Aerosols from Nature)." *Atmospheric Chemistry and Physics* 6: 3181–3210. https://doi.org/10.5194/acp-6-3181-2006.

Hicks, B. B., J. J. DeLuisi, and D. R. Matt, 1996. "The NOAA Integrated Surface Irradiance Study (ISIS)—A New Surface Radiation Monitoring Program." *Bulletin of the American Meteorological Society* 77: 2857–2864. https://doi.org/10.1175/1520-0477(1996)077<2857:TNISIS>2.0.CO;2.

Hill, J., J. Kern, D. E. Rupp, N. Voisin, and G. Characklis. 2021. “The Effects of Climate Change on Interregional Electricity Market Dynamics on the U.S. West Coast.” *Earth’s Future* 9 (12). https://doi.org/10.1029/2021EF002400.

Holben, B. N., J. P. Buis, A. Setzer, T. F. Eck, I. Slutsker, D. Tanre, E. Vermote, J. A. Reagan, Y. J. Kaufman, T. Nakajima, F. Lavenu, I. Jankowiak, and A. Smirnov. 1998. “AERONET—A Federated Instrument Network and Data Archive for Aerosol Characterization, Remote Sensing of Environment, Volume 66, Issue 1. https://doi.org/10.1016/S0034-4257(98)00031-5.

Hong, S., Y. Noh, and J. Dudhia. 2006. “A New Vertical Diffusion Package With an Explicit Treatment of Entrainment Processes.” *Monthly Weather Review* 134(9): 2318-2341.

Ibanez, E., G. Brinkman, M. Hummon, and D. Lew. 2013. “Solar Reserve Methodology for Renewable Energy Integration Studies Based on Sub-hourly Variability Analysis: Preprint.” Presented at the Second Annual International Workshop on Integration of Solar Power into Power Systems, November 12–13, Lisbon, Portugal. Golden, CO: National Renewable Energy Laboratory. NREL/CP-5500-56169.

Jaglom, W. S., J. R. McFarland, M. F. Colley, C. B. Mack, B. Venkatesh, R. L. Miller, J. Haydel, P. A. Schultz, B. Perkins, J. H. Casola, J. A. Martinich, P. Cross, M. J. Kolian, and S. Kayin. 2014. “Assessment of Projected Temperature Impacts From Climate Change on the U.S. Electric Power Sector Using the Integrated Planning Model®.” *Energy Policy* 73: 524–539. https://doi.org/10.1016/j.enpol.2014.04.032.

Jiménez, P. A., J. Dudhia, J. F. González-Rouco, J. Navarro, J. P. Montávez, and E. García-Bustamante. 2012. “A Revised Scheme for the WRF Surface Layer Formulation.” *Monthly Weather Review* 140 (3): 898–918.

Juliano, T. W., P. A. Jiménez, B. Kosović, T. Eidhammer, G. Thompson, L. K. Berg, J. Fast, A. Motley, and A. Polidori. 2022. “Smoke From 2020 United States Wildfires Responsible for Substantial Solar Energy Forecast Errors.” *Environmental Research Letters* 17. https://doi.org/10.1088/1748-9326/ac5143.

Li, Y., L. J. Mickley, P. Liu, and J. O. Kaplan. 2020. “Trends and Spatial Shifts in Lightning Fires and Smoke Concentrations in Response to 21st Century Climate Over the National Forests and Parks of the Western United States.” *Atmospheric Chemistry and Physics* 20: 8827–8838. https://doi.org/10.5194/acp-20-8827-2020.

Lin, C. A., Y. Zhang, G. Heath, D. K. Henze, M. Sengupta, and C. H. Lu. 2023. Improvement of Aerosol Optical Depth Data for Localized Solar Resource Assessment. *Solar Energy* 249: 457–466. https://doi.org/10.1016/J.SOLENER.2022.11.047.

Littell, J. S., D. McKenzie, H. Y. Wan, and S. A. Cushman. 2018. “Climate Change and Future Wildfire in the Western United States: An Ecological Approach to Nonstationarity.” *Earth’s Future* 6: 1097–1111. https://doi.org/10.1029/2018EF000878.

Liu, J. C., L. J. Mickley, M. P. Sulprizio, F. Dominici, X. Yue, K. Ebisu, G. B. Anderson, R. F. A. Khan, M. A. Bravo, and M. L. Bell. 2016. "Particulate Air Pollution From Wildfires in the Western U.S. Under Climate Change." *Climate Change* 138: 655–666. https://doi.org/10.1007/s10584-016-1762-6.

Liu, Yongqiang, Yang Liu, J. Fu, C. E. Yang, X. Dong, H. Tian, B. Tao, J. Yang, Y. Wang, Y. Zou, and Z. Ke. 2022. "Projection of Future Wildfire Emissions in Western USA Under Climate Change: Contributions From Changes in Wildfire, Fuel Loading and Fuel Moisture." *International Journal of Wildland Fire* 31: 1–13. https://doi.org/10.1071/WF20190.

Liu, Z., and M. C. Wimberly. 2016. "Direct and Indirect Effects of Climate Change on Projected Future Fire Regimes in the Western United States." *Science of the Total Environment* 542: 65–75. https://doi.org/10.1016/j.scitotenv.2015.10.093.

Mann, M. L., E. Batllori, M. A. Moritz, E. K. Waller, P. Berck, A. L. Flint, L. E. Flint, and E. Dolfi. 2016. "Incorporating Anthropogenic Influences Into Fire Probability Models: Effects of Human Activity and Climate Change on Fire Activity in California." *PLoS One* 11: 1–21. https://doi.org/10.1371/journal.pone.0153589.

Mlawer, E. J., S. J. Taubman, P. D. Brown, M. J. Iacono, and S. A. Clough. 1997. "Radiative Transfer for Inhomogeneous Atmospheres: RRTM, a Validated Correlated-k Model for the Longwave." *Journal of Geophysical Research* 102 (D14): 16663–16682. https://doi.org/10.1029/97JD00237.

Pfister, G. G., J. Avise, C. Wiedinmyer, D. P. Edwards, L. K. Emmons, G. D. Diskin, J. Podolske, and A. Wisthaler. 2011. "CO Source Contribution Analysis for California During ARCTAS-CARB." *Atmospheric Chemistry and Physics* 11: 7515–7532. https://doi.org/10.5194/acp-11-7515-2011.

Pierce, J. R., M. V. Martin, and C. L. Heald. 2017. *Estimating the Effects of Changing Climate on Fires and Consequences for U.S. Air Quality, Using a Set of Global and Regional Climate Models–Final Report to the Joint Fire Science Program*. Fort Collins, CO: Fort Collins Joint Fire Science Program.

Randles, C. A., A. M. da Silva, V. Buchard, P. R. Colarco, A. Darmenov, R. Govindaraju, A. Smirnov, B. Holben, R. Ferrare, J. Hair, Y. Shinozuka, and C. J. Flynn. 2017. "The MERRA-2 Aerosol Reanalysis, 1980 Onward. Part I: System Description and Data Assimilation Evaluation." *Journal of Climate* 30: 6823–6850. https://doi.org/10.1175/JCLI-D-16-0609.1.

Schoennagel, T., J. K. Balch, H. Brenkert-Smith, P. E. Dennison, B. J. Harvey, M. A. Krawchuk, N. Mietkiewicz, P. Morgan, M. A. Moritz, R. Rasker, M. G. Turner, and C. Whitlock. 2017. "Adapt To More Wildfire in Western North American Forests as Climate Changes." Proceedings of the National Academy of Sciences of the United States of America 114: 4582–4590. https://www.pnas.org/doi/full/10.1073/pnas.1617464114.

Seidl, R., D. Thom, M. Kautz, D. Martin-Benito, M. Peltoniemi, G. Vacchiano, J. Wild, D. Ascoli, M. Petr, J. Honkaniemi, M. J. Lexer, V. Trotsiuk, P. Mairota, M. Svoboda, M. Fabrika, T. A. Nagel, and C. P. O. Reyer. 2017. "Forest Disturbances Under Climate Change." *Nature Climate Change* 7: 395–402. https://doi.org/10.1038/nclimate3303.

Sengupta, M., and Wagner, M. J. M. 2011. Impact of Aerosols on Atmospheric Attenuation Loss in Central Receiver Systems. Proceedings of the 2011 SolarPACES International Symposium, (August), 6. Retrieved from http://www.nrel.gov/docs/fy11osti/52487.pdf

Sengupta, M., Y. Xie, A. Lopez, A. Habte, G. Maclaurin, and J. Shelby. 2018. "The National Solar Radiation Data Base (NSRDB)." *Renewable and Sustainable Energy Reviews* 89: 51–60. https://doi.org/10.1016/j.rser.2018.03.003.

Sigrin, Benjamin, Michael Gleason, Robert Preus, Ian Baring-Gould, and Robert Margolis. 2016. *Distributed Generation Market Demand Model (dGen): Documentation*. Golden, CO: National Renewable Energy Laboratory. NREL/TP-6A20-65231. https://www.nrel.gov/docs/fy16osti/65231.pdf.

Spracklen, D. V, L. J. Mickley, J. A. Logan, R. C. Hudman, R. Yevich, M. D. Flannigan, and A. L. Westerling. 2009. "Impacts of Climate Change From 2000 to 2050 on Wildfire Activity and Carbonaceous Aerosol Concentrations in the Western United States." *Journal of Geophysical Research* 114: 1–17. https://doi.org/10.1029/2008JD010966.

Su, Y., J. D. Kern, P. M. Reed, and G. W. Characklis. 2020. "Compound Hydrometeorological Extremes Across Multiple Timescales Drive Volatility in California Electricity Market Prices and Emissions." *Applied Energy* 276. https://doi.org/10.1016/j.apenergy.2020.115541.

Thompson, G., R. M. Rasmussen, and K. Manning. 2004. "Explicit Forecasts of Winter Precipitation Using an Improved Bulk Microphysics Scheme. Part I: Description and Sensitivity Analysis." *Monthly Weather Review* 132 (2): 519–542, https://doi.org/10.1175/1520-0493(2004)132<0519:EFOWPU>2.0.CO;2.

Val Martin, M., C. L. Heald, J. F. Lamarque, S. Tilmes, L. K. Emmons, and B. A. Schichtel. 2015. "How Emissions, Climate, and Land Use Change Will Impact Mid-Century Air Quality Over the United States: A Focus on Effects at National Parks." *Atmospheric Chemistry and Physics* 15, 2805–2823. https://doi.org/10.5194/acp-15-2805-2015.

Vimmerstedt, Laura J., Sertaç Akar, Chad Augustine, Philipp Beiter, Wesley Cole, David Feldman, Parthiv Kurup, Eric Lantz, Robert Margolis, Ashwin Ramdas, Tyler Stehly, Craig Turchi, and Debo Oladosu. 2019. "2019 Annual Technology Baseline." Presented August 22, 2019. Golden, CO: National Renewable Energy Laboratory. NREL/PR-6A20-74273. https://www.nrel.gov/docs/fy19osti/74273.pdf.

Westerling, A. L. R. 2016. “Increasing Western U.S. Forest Wildfire Activity: Sensitivity to Changes in the Timing of Spring.” *Philosophical Transactions of the Royal Society B: Biological Sciences* 371. https://doi.org/10.1098/rstb.2015.0178.

Westerling, A. L., B. P. Bryant, H. K. Preisler, T. P. Holmes, H. G. Hidalgo, T. Das, and S. R. Shrestha. 2011. “Climate Change and Growth Scenarios for California Wildfire.” *Climate Change* 109, 445–463. https://doi.org/10.1007/s10584-011-0329-9.

Wiedinmyer, C., S. K. Akagi, R. J. Yokelson, L. K. Emmons, J. A. Al-Saadi, J. J. Orlando, and A. J. Soja. 2011. “The Fire INventory from NCAR (FINN): A High Resolution Global Model to Estimate the Emissions From Open Burning.” *Geoscientific Model Development* 4: 625–641, https://doi.org/10.5194/gmd-4-625-2011.

Yue, X., L. J. Mickley, and J. A. Logan. 2014. “Projection of Wildfire Activity in Southern California in the Mid-Twenty-First Century.” *Climate Dynamics* 43: 1973–1991. https://doi.org/10.1007/s00382-013-2022-3.

Yue, X., L. J. Mickley, J. A. Logan, and J. O. Kaplan. 2013. “Ensemble Projections of Wildfire Activity and Carbonaceous Aerosol Concentrations Over the Western United States in the Mid-21st Century.” *Atmospheric Environment* 77: 767–780. https://doi.org/10.1016/j.atmosenv.2013.06.003.

Zhao, Y., A. E. Brooks, and X. Du. 2021. “The Impact of Natural Disaster on Wholesale Electricity Market: The Case of Hurricane Harvey in ERCOT.” MATPOWER. https://matpower.org.